ADVANCED THERAPEUTICS
www.advtherap.com

Redox-Triggered Nanomedicine via Lymphatic Delivery: Inhibition of Melanoma Growth by Ferroptosis Enhancement and a Pt(IV)-Prodrug Chemoimmunotherapy Approach

*Marc Bilbao-Asensio, Ane Ruiz-de-Angulo, Amaia Garaikoetxea Arguinzoniz, James Cronin, Jordi Llop, Aintzane Zabaleta, Saul Michue-Seijas, Dominika Sosnowska, James N. Arnold, and Juan C. Mareque-Rivas**

The efficacy of therapies is often hampered by limited tumor drug accumulation achieved through their intravenous administration, and by the lack of selectivity in targeting and killing cancer cells. Amplification of tumor redox stress and ferroptotic cell death to achieve selective killing of cancer cells using iron-containing agents has attracted considerable interest. However, these agents need high doses and multiple injection regimens and have limited success in the treatment of cancers such as melanoma. Melanoma often metastasizes via lymphatic vessels, where the metastasizing cells experience less redox stress and are protected from ferroptosis. Here it is shown that phospholipid-modified Pt(IV) prodrug-loaded iron oxide nanoparticle (IONP)-filled micelles (mIONP-PL-Pt(IV)), which integrate redox reactivity and iron-enabled catalytic therapeutic features with effective nanoparticle-assisted lymphatic delivery, provide significantly enhanced suppression of melanoma tumor growth compared to cisplatin-based chemotherapy and IONP treatments. Peroxidase-like activity, redox-triggered release of cisplatin, and reactivity with hydrogen peroxide and ascorbic acid are contributors toward the induction of a combined ferroptosis-based and cisplatin anti-melanoma treatment. Treatment with mIONP-PL-Pt(IV) provides significant tumor control using cumulative treatment doses 10–100-fold lower than reported in intravenously administered treatments. This work demonstrates the potential of enhancing chemotherapeutic and iron-based catalytic nanomedicine efficacy exploiting nanoparticle-enabled lymphatic trafficking.

1. Introduction

Whereas platinum-based chemotherapeutics are still considered the "penicillin of cancer,"[1] the clinical use of iron oxide nanoparticles (IONPs) is mainly restricted to iron deficiency therapeutics and contrast agents in magnetic resonance imaging (MRI).[2,3] In the light of recent findings related to oxidative stress-mediated cell death, and ferroptosis as a novel therapeutic strategy for cancer, here we show that the extension of the configuration of these systems as oxidative stress inducers and redox-triggered cancer therapeutics via lymphatic drug delivery offers intriguing new possibilities in cancer nanomedicine. We report phospholipid-modified platinum(IV) prodrug-coated IONP micelles (mIONP-PL-Pt(IV)) that, based on a combination of therapeutic features resulting from iron and Pt(IV)-enabled redox processes and nanoparticle-assisted lymphatic delivery, provide significantly enhanced suppression of melanoma tumor growth compared to cisplatin-based chemotherapy and chemoimmunotherapy.

Platinum-based chemotherapy exploits the ability of Pt(II) centers to form

M. Bilbao-Asensio, S. Michue-Seijas, J. C. Mareque-Rivas
Department of Chemistry
Swansea University
Singleton Park, Swansea SA2 8PP, UK
E-mail: juan.mareque-rivas@swansea.ac.uk

The ORCID identification number(s) for the author(s) of this article can be found under https://doi.org/10.1002/adtp.202200179

DOI: 10.1002/adtp.202200179

A. Ruiz-de-Angulo, A. G. Arguinzoniz
CIC biomaGUNE
Paseo Miramón 182, San Sebastián 20014, Spain

J. Cronin
Swansea University Medical School
Singleton Park, Swansea SA2 8PP, UK

J. Llop
Radiochemistry and Nuclear Imaging Laboratory
CIC biomaGUNE
Paseo Miramón 182, San Sebastián 20014, Spain

platinum-DNA adducts via coordination of the N7 atoms of purine bases causing cross-links on DNA, which by activating DNA damage recognition and repair pathways ultimately leads to cell death.[4,5] In testicular cancer the outcomes of cisplatin treatment are impressive, turning a negligible cure rate with 90% mortality within a year before cisplatin FDA approval in 1978 into the current cures achieved in >95% of all patients.[6] However, the vast majority of the Pt(II) drug administered to the patient does not end up platinating the DNA of cancer cells due to a lack of tumor targeting, which leads to off-target drug effects that can cause severe toxicity. Furthermore, cancer cells can exhibit resistance and develop protective mechanisms against these treatments.[4]

In the past decade, however, a major shift in platinum-based drug design has occurred with the development of kinetically inert octahedral Pt(IV) prodrugs. These compounds can be converted and activated in situ by a redox mechanism to the corresponding square-planar Pt(II) drugs with release of two axial ligands.[7] This chemical strategy allows better tolerated treatments together with the adoption of different approaches for improved drug delivery, including use of specialized delivery devices such as nanoparticles (NPs) and endogenous proteins (e.g., human serum albumin (HSA)).[7,8] A wide range of NP-Pt(IV) and NP-Pt(II) systems were developed and tested aiming to improve drug accumulation in the tumor. However, many relied on the enhanced permeability and retention (EPR) effect achieved by intravenous administration, an approach which, although promising, has major limitations and has led to major clinical failures in cancer nanomedicine.[9,10]

Metastatic melanoma continues to be among the most aggressive and difficult to treat types of cancer. Even in the immunotherapy era, for many patients with this disease the outcome remains bleak.[11] Unfortunately, chemotherapy approaches, including cisplatin and all the other platinum-based drugs and nanomedicines, remain extremely ineffective for melanoma treatment due to the drug resistance characteristics of the disease.[12] New strategies are therefore needed to enhance and expand the activity and delivery of platinum-based treatments in melanoma and other therapy-resistant cancers.

Although cancer metastasis can occur through the blood, it is a highly inefficient process in which few cancer cells survive.[13] Epithelial cancers and melanoma are known to metastasize to draining lymph nodes (LNs) mainly via lymphatic vessels,[14] and regional LN metastasis is one of the most important predictors of distant metastasis and death.[15] The biological mechanisms that allow tumor cells to survive and proliferate when exploiting the lymphatic system are not well-known. However, recent evidence points to their unique enhanced ability to withstand oxidative stress, which as a critical determinant of cell fate provides a potential therapeutic target.[16,17] A new paradigm has emerged with the recent discovery of ferroptosis, a form of regulated cell death triggered upon extensive lipid peroxidation catalyzed by iron.[18–20] Since cancer cells are more susceptible to oxidative damage than normal cells and have greater demand for iron, in situ release of reactive oxygen species (ROS) and ferroptosis-inducing drugs are viewed as highly promising anticancer therapeutic strategies.[21,22] Indeed, various IONPs have been investigated as redox-triggered ferroptosis-inducing agents,[23] showing an ability to exploit the tumor cell-derived H_2O_2 to generate ROS and ultimately trigger ferroptosis.[23–25] Moreover, the iron oxide particle surface can exhibit enzyme-mimetic catalytic activity and take advantage of in situ Fenton-like reactions with H_2O_2 to generate cytotoxic hydroxyl radicals for chemodynamic therapy (CDT).[26–31] Together with the elevated content of H_2O_2 in the tumor microenvironment (TME), this strategy offers the intriguing possibility of exploiting the local TME for triggering physiological cancer-specific cell death.[32,33] However, a major challenge lies in achieving significant therapeutic effects without requiring high dosage of IONPs. This challenge has been tackled in different ways recently, ranging from incorporation of glutathione (GSH) inhibitors[34] to H_2O_2 encapsulation or by ensuring "self-supply" of O_2 and H_2O_2[35,36] and IONP-mediated lipid peroxidation.[37] Increased drug accumulation in the tumor has also been possible to some extent by exploiting the magnetic properties of the IONPs.[38,39] However, like the NP-Pt(II) and NP-Pt(IV) systems, these IONPs were designed and optimized for intravenous administration of the therapy, which also limits the ability to target melanoma cells in lymph fluid and in the tumor draining LNs (TDLNs). This is an important design drawback given that the LNs provide a microenvironment distinct from the primary tissue,[40] and one that promotes the survival of metastasizing melanoma cells and their resistance to ferroptosis.[41] However, so far, little or no attention has been devoted to lymphatic delivery of both platinum-based chemotherapy[42,43] and of nanomaterials for ferroptosis/ROS-mediated therapy. From an immunologic perspective, cancer cell death by ferroptosis and cisplatin offers additional potential for eliciting effective antitumor immune responses to control residual tumor cells. Hence, our approach here integrates lymphatic delivery and TDLN targeting with a strategy that enhances the immunostimulatory capacity of the mIONP-based therapy system based on "stealth" hydrophobicity,[44–47] to potentially make the destroyed cancer cells more "visible" to dendritic cells that present the tumor antigens to T cells. Our recent studies have indeed shown that these mIONPs as carriers of tumor antigens and Toll-like receptor ligands drive potent and effective therapeutic immune responses to cancer.[45,48–51] In this work we show that the lipid/phospholipid-rich nanoparticle formulation mIONP-PL-Pt(IV) provides remarkable therapeutic efficacy at relatively low non-toxic doses (less than 1% of the allometric dose used in the clinic for platinum-based drugs) by exploiting the i) redox catalytic activity of the iron oxide core, ii) the P(IV) prodrug approach, iii) nanoparticle-enabled lymphatic delivery, iv) the immunogenicity of "stealth" hydrophobic portions, and v) the recently discovered susceptibility of therapy-resistant melanoma cells to ferroptosis (**Scheme 1**). mIONP-PL-Pt(IV)-based treatments reduce tumor burden and achieve significantly

A. Zabaleta
Clinica Universidad de Navarra
Centro de Investigación Médica Aplicada (CIMA)
IdiSNA
Instituto de Investigación Sanitaria de Navarra
Pamplona 31009, Spain
D. Sosnowska, J. N. Arnold
School of Cancer and Pharmaceutical Sciences
King's College London
London SE1 1UL, UK

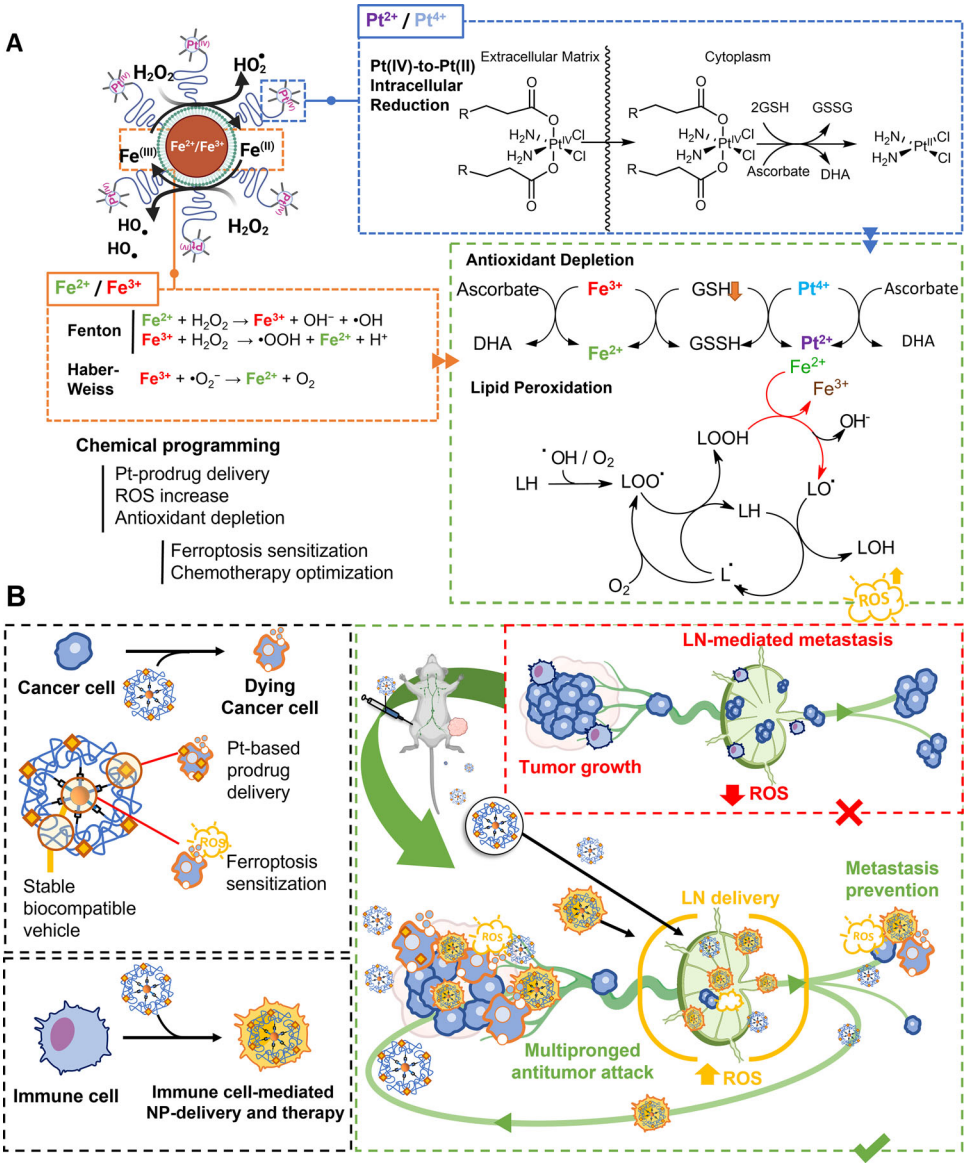

Scheme 1. Reactivity, redox-triggered therapy, and drug delivery features of mIONP-PL-Pt(IV). A) The Pt(IV) prodrug and IONP core are chemically programmed to release cisplatin and, via the Fenton reaction and peroxidase-like activity, to produce ROS and induce lipid peroxidation. B) The size-selected mIONP-PL-Pt(IV) enables direct and indirect (immune cell-mediated) cancer cell killing through the delivery of the therapeutic compound to the lymph nodes, where lower oxidative stress level of melanoma cells promotes the survival of metastasizing melanoma cells and their resistance to ferroptosis.

improved therapeutic outcomes in comparison to cisplatin without apparent toxicity, while providing functionality for multimodal monitorable biodistribution and multimodal therapy combination against highly aggressive melanoma.

2. Results and Discussion

2.1. Synthesis and Characterization of a Dual-Acting Cytotoxic and Pro-Ferroptotic Anti-Cancer Nanoparticle: mIONP-PL-Pt(IV)

Adopting the Pt(IV) prodrug approach, the cisplatin prodrug *cis,cis,trans*-[$Pt(NH_3)_2Cl_2(O_2CCH_2CH_2CO_2H)_2$] was selected for attachment and delivery using IONP-core PEGylated phospholipid micelles. Synthesis of the PEGylated PL-Pt(IV) was confirmed by UPLC-ESI-MS/MS, ^{1}H NMR, and XPS characterization (Figures S1 and S2, Supporting Information), complementing and showing consistency with previous studies.[52–54] Methods for self-assembly of amphiphiles and nanoparticles and thin dry-film hydration were used to obtain the mIONP-PL-Pt(IV) with a 1:2.5 ratio (w:w) of hydrophobic IONPs and PEGylated PL-Pt(IV) (**Figure 1**A). IONP-filled micelle formation yielded nanoparticles with excellent colloidal stability in water/PBS with a size of 30 nm, which is ideal for lymphatic trafficking (Figure 1B).[55] TEM imaging confirmed absence of aggregates (Figure 1C and Figure S1, Supporting Information). The cisplatin prodrug loading and its ability to release cisplatin by

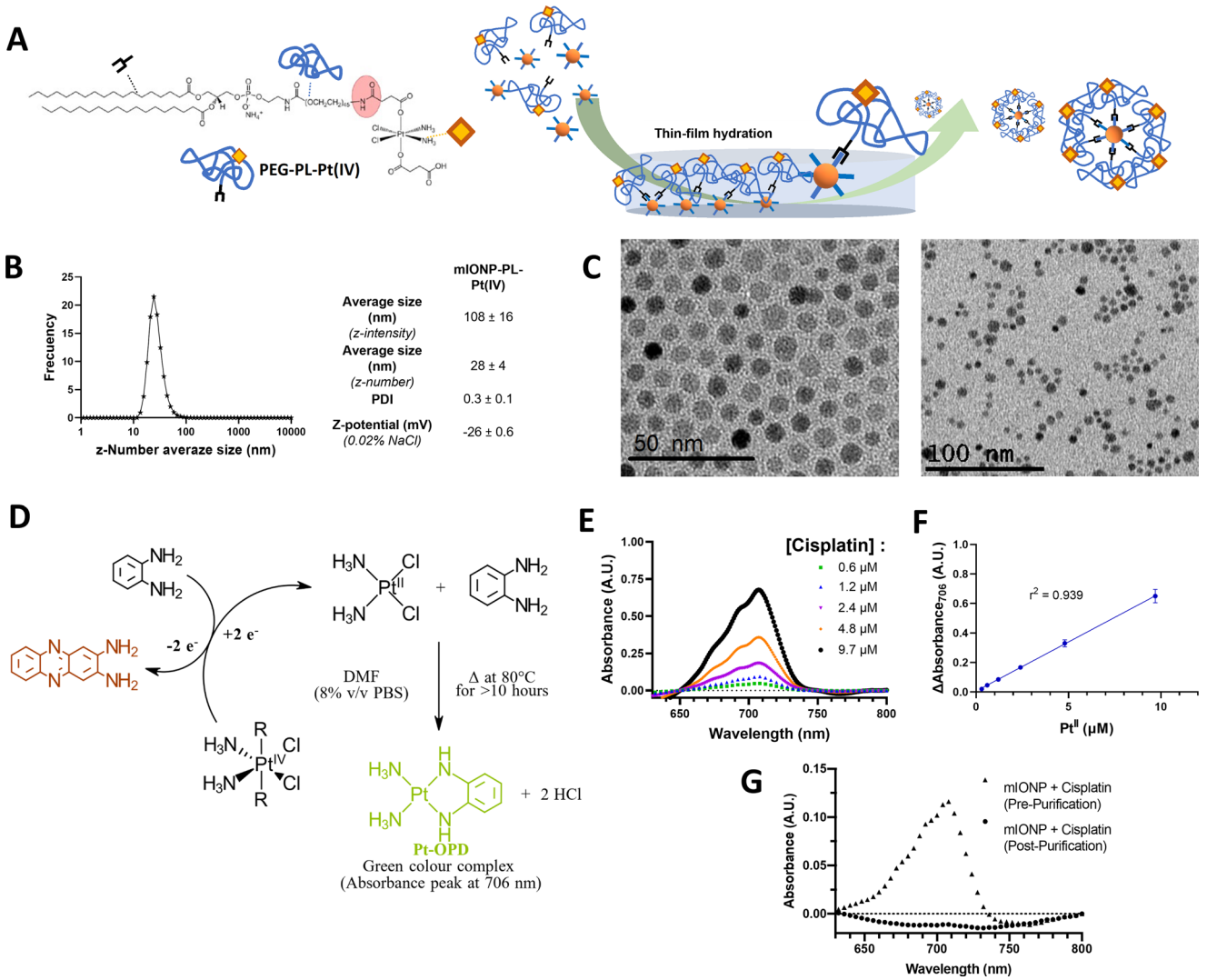

Figure 1. Assembly and characterization of mIONP-PL-Pt(IV). A) Schematic representation of the formation of mIONP-PL-Pt(IV) by self-assembly of hydrophobic IONPs and PL-PEG-Pt(IV) by thin-film hydration. B) Size and zeta-potential characterization of mIONP-PL-Pt(IV). Values as mean ± SEM from at least three independent experiments. C) Representative TEM images of the IONPs and mIONP-PL-Pt(IV). D) OPD-mediated Pt(IV) reduction and formation of green Pt(II)-OPD/OPDox complexes. E) UV–vis spectra of complexes formed by reaction of OPD with cisplatin at increasing [Pt] concentrations, F) linear fit of the calibration curve. G) UV–vis spectra formed by reaction of OPD with mIONPs ([IONP] = 1 μM) previously treated with cisplatin ([Pt] = 350 μM) prior and after purification, confirming that mIONPs do not bind cisplatin and confirming mIONP-PL-Pt(IV) prodrug covalent attachment and OPD-induced cisplatin release.

a redox mechanism could be detected and quantified by a colorimetric strategy. In this strategy the Pt(IV)-induced oxidation of o-phenylenediamine (OPD) to 2,3-diaminophenazine (usually called OPDox) was coupled with cisplatin generation (OPD acting as reducing agent) and OPD/OPDox coordination to the Pt(II) center of the released drug. The ortho-phenylenediamine ligands substitute the labile chloride ligands at the Pt(II) center to form Pt(II) complexes with a strong absorbance peak at 706 nm (Figure 1D–G).[56] To investigate if mIONP has some intrinsic cisplatin binding ability and therefore could act as drug nanocarriers, mIONPs obtained by encapsulation with PEGylated phospholipid were incubated with cisplatin solutions. After removal of the unbound cisplatin by centrifugation/filtration they were reacted with OPD. The results showed that mIONPs are not able to bind to cisplatin and confirmed that the Pt(II) complexes detected in the solutions of mIONP-PL-Pt(IV) were all released from the covalently conjugated Pt(IV) complexes (Figure 1G). Pt(IV) prodrug reduction to cisplatin is not completely quantitative (81 ± 2% yield; $N = 3$). This is consistent with recent research, which has indicated that Pt(IV) prodrug reduction results in the formation of different complexes and that the assumption of clean axial ligand loss needs to be reassessed.[57]

2.2. Cell Uptake and Cytotoxic Effects of mIONP-PL-Pt(IV) on the Melanoma Cells

To investigate the uptake and cytotoxicity in melanoma cells, we first synthesized mIONP-PL-Pt(IV) with rhodamine-labeled

fluorescent phospholipids (mIONP-PL-Pt(IV)/Rho). Incorporation of the rhodamine fluorophore was evident by a noticeable absorption peak at 570 nm (Figure S3, Supporting Information). The mIONP-PL-Pt(IV)/Rho had physical properties similar to those of mIONP-PL-Pt(IV) lacking the fluorescently labeled phospholipid. We confirmed the efficient internalization of mIONP-PL-Pt(IV)/Rho incubated with B16-F10 melanoma cells, which localize in the cytoplasm (Figure S4A,B, Supporting Information). When we investigated melanoma cell killing, mIONP-PL-Pt(IV) proved to be as effective as cisplatin promoting tumor cell death, with a more than 10-fold increase in the IC_{50} compared to the Pt(IV) prodrug alone or mIONP + Pt(IV) prodrug (Figure S4C, Supporting Information). This result demonstrated the importance of the mIONP nanocarrier for the Pt(IV) prodrug delivery. These results are in agreement with our previous studies showing that mIONP-PL-Pt(IV) facilitated increased intracellular platinum accumulation as well as cytotoxicity comparable to cisplatin in various human cancer cell lines.[58]

2.3. Intrinsic NP Peroxidase-Like Activity to Facilitate Tumor-Specific Activation

The peroxidase-like activity of mIONP-PL-Pt(IV) was assayed by the colorimetric reaction of H_2O_2 with the peroxidase substrate 3,3′,5,5′-tetramethylbenzidine (TMB), which upon oxidation turns blue ($\varepsilon_{652} = 3.9 \times 10^4\ M^{-1}\ cm^{-1}$, **Figure 2**B). mIONP-PL-Pt(IV) efficiently catalyzed the peroxidative reactions at the acidic conditions found in the TME and endosomal compartments reached by the mIONPs inside the cells. UV–vis absorption time course curves, the kinetic parameters obtained by Lineweaver–Burk plots, and fitting the catalytic reaction curves to the Michaelis–Menten rate equation indicated that the mIONP-PL-Pt(IV) had higher peroxidase-like activity than the Pt(IV)-free mIONPs under the same conditions (Figure 2C). The low apparent K_M (H_2O_2) values for mIONP-PL-Pt(IV) is indicative of the IONP-core lipid nanoparticle-based nanozymes having 10–30-fold higher affinity for the H_2O_2 substrate than natural peroxidases like horseradish peroxidase (HRP). This is consistent with results obtained with other peroxidase-like artificial nanozymes.[55] The results also indicate that the redox active Pt(IV) prodrug participates in the oxidation of TMB, which is both mediated by the iron from the nanoparticle cycling between the +III and +II oxidation states and the reduction of the Pt(IV) prodrug complexes to the Pt(II) drugs (Figure 2A). Hence, the mIONP-PL-Pt(IV) system enables coupling peroxidative activity with cisplatin prodrug activation and release at the acidic pH levels found after tumor cell uptake.

This result is also important given that lipid peroxidation level is one of the most critical indicators of ferroptosis.[59] Cisplatin-induced lipid peroxidation is known to be involved in nephrotoxicity,[60] but some evidence suggests it can induce similar oxidative damage to tumor cells.[61] To study the possible contribution of peroxidase-like activity and ferroptosis in the cancer cell killing effects of mIONP-PL-Pt(IV), we first measured lipid peroxidation in the melanoma cells using Liperfluo, which when reacting with hydroperoxides yields the fluorescent Liperfluo-Ox product (Figure 2D). The flow cytometry studies showed that the presence of hydroperoxide lipids in melanoma cells treated with mIONP-PL-Pt(IV) was higher than in cells treated with the Pt(IV)-free mIONPs (Figure 2E).

It is known that inflammatory cells and fast-proliferating tumor cells generate large quantities of H_2O_2 in the TME or during immunity against disease (≈50–100 μM).[62,63] Therefore, we then investigated the effect of exogenously applied H_2O_2 on melanoma cell survival. As shown in **Figure 3**A, treatment with 50 or 75 μM H_2O_2 for 24 h resulted in ≈20% cell death of the B16-F10 cells. We sought to identify if the H_2O_2-induced cell death could be enhanced by mIONP-PL-Pt(IV) treatment ([Fe] = 500 μM; [Pt] = 10 μM). For this, melanoma cells were first exposed to the treatments for 24 h, the non-internalized drugs were removed, and the cells were exposed to H_2O_2 for another 24 h. Indeed, the pre-treatment with mIONP-PL-Pt(IV) induced higher levels of melanoma cell death (60 ± 8%) than the mIONP pre-treatment (43 ± 4%) and equivalent to mIONP + cisplatin co-pre-treatments (62 ± 4%) (Figure 3A) when exposed to 75 μM H_2O_2. The data normalized to absence of H_2O_2 treatments shows that the mIONP-PL-Pt(IV) system induces sensitization to the H_2O_2-induced cell death at 75 μM H_2O_2 (Figure 3B).

Finally, we also explored the potential of mIONP-PL-Pt(IV) treatment combined with ascorbic acid (AA; vitamin C), a natural compound with important redox functions and the ability to both produce H_2O_2 and affect iron metabolism targeting multiple critical pathways and cancer-specific vulnerabilities.[64] Over the past decade, a growing number of studies have shown that millimolar concentrations of pharmacological AA can selectively kill cancer cells to induce antitumor activity across multiple tumor types. An important breakthrough has been in new studies that show that these high concentrations of AA can be achieved by intravenous delivery, they are well tolerated and reduce the toxicity of chemotherapy.[65] As a result high-dose, intravenous AA administration is generating new excitement and promising possibilities for treating various types of cancer both as a monotherapy and in combination therapy.[66,67] On the other hand, the reduction of inert platinum (IV) prodrug complexes to platinum (II) by biological reducing agents (e.g., ascorbate, glutathione) provides a mechanism for chemotherapy drug release and activation.[7] A screening of AA concentrations (0–40 mM) revealed that short 1 h treatments were enough to trigger cytotoxic effects in the melanoma cells (Figure 3C). The AA-induced cytotoxicity was then evaluated following pre-treatment with the mIONP, Pt(IV) prodrug, cisplatin, and mIONP-PL-Pt(IV) for 24 h. The melanoma cells were treated with these systems for 24 h, the non-internalized drugs were removed, and then treated with 5 mM AA for 1 h. The results showed the cytotoxicity induced with 5 mM AA was enhanced according to the following trend: mIONP-PL-Pt(IV) > cisplatin > mINOP > Pt(IV) prodrug (Figure 3D).

The stronger effect induced by mIONP-PL-Pt(IV) can be explained by the Fe(II)/Fe(III) driven iron oxide nanozyme activity, facilitated Pt(IV) intracellular accumulation and Pt(IV)-to-Pt(II) intracellular activation, further assisted by the integrated prooxidant role of AA.

Mechanistically, the mIONP-PL-Pt(IV) in the presence of H_2O_2 can kill the melanoma cells by several mechanisms that complement/reinforce each other and are enabled by the nanoparticle-driven chemical reactivity (Figure 3E).

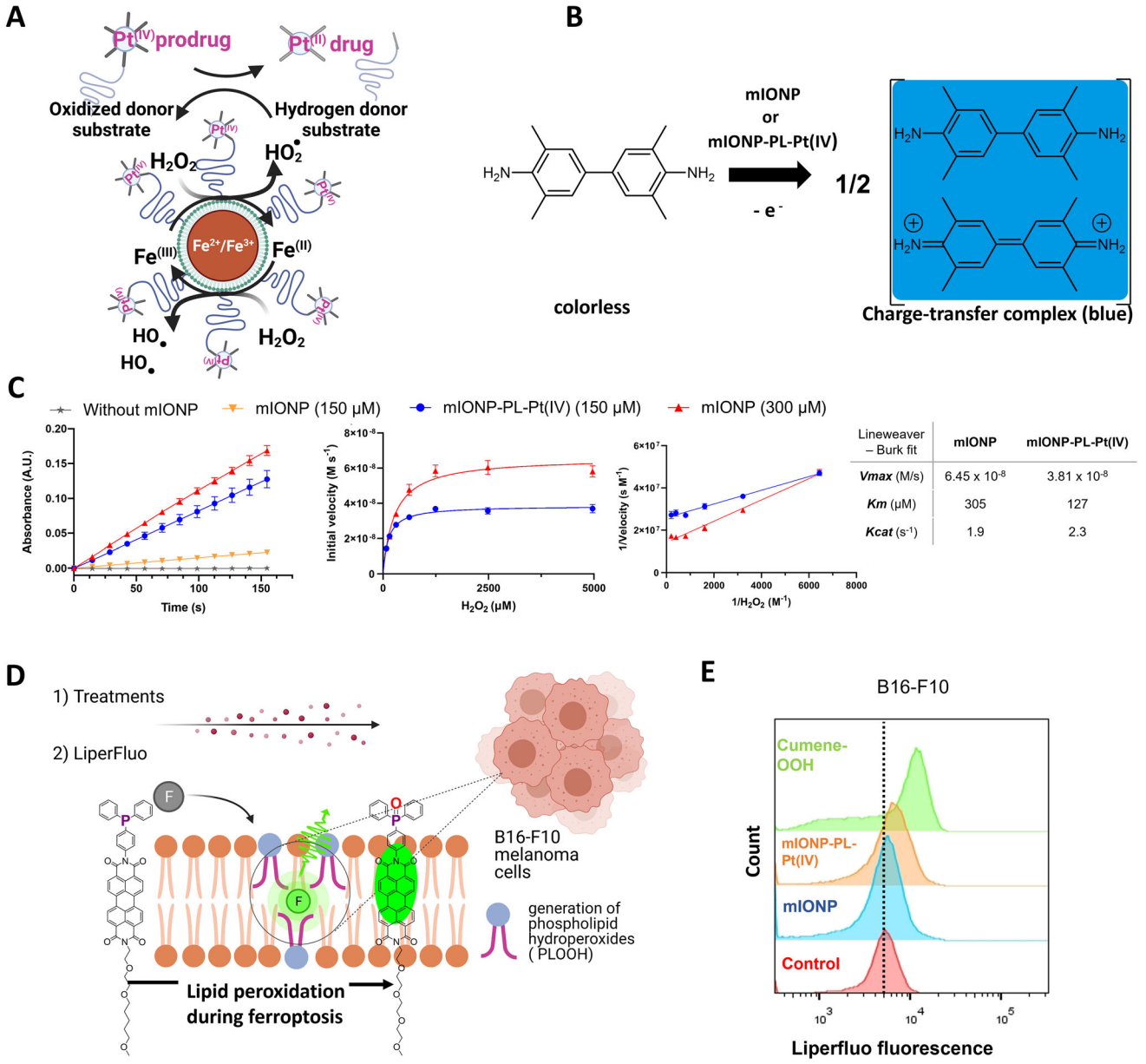

Figure 2. Peroxidase-like and lipid peroxidation activity of mIONP-PL-Pt(IV). A) Schematic illustration of the peroxidase-like catalytic process of mIONP-PL-Pt(IV) acting as nanozyme. B,C) Catalytic oxidation of TMB with H_2O_2 using mIONP-PL-Pt(IV) versus Pt(IV) prodrug-free mIONPs, showing the Michaelis–Menten and Lineweaver–Burk plots and kinetic parameters. D) Reaction of Liperfluo with hydroperoxide lipids to generate fluorescence Liperfluo-Ox. E) B16-F10 cells incubated with IONPs ([Fe] = 500 μM; [Pt] = 10 μM) for 24 h. Representative flow cytometry histograms are shown to demonstrate the increase in lipid peroxides with Liperfluo signals (cells treated with cumene hydroperoxide (100 μM, 1 h) are used as positive control).

First, H_2O_2 can freely diffuse across cell membranes and interact with ferrous iron and via Fenton chemistry produce the highly destructive and short-lived hydroxyl radical (HO•), which causes damage to cellular proteins, lipids, and nucleic acids, which, in turn, leads to both apoptosis and ferroptosis in tumor cells.[22,68,69] Hypoxia-induced superoxide production, leads to the generation of intracellular H_2O_2 through the catalytic activity of superoxide dismutase (SOD).[70] Second, the IONP-delivered Fe(II) can react with H_2O_2, to generate the damaging HO•. To perpetuate this reaction, ascorbate can donate electrons to Fe(III) to regenerate Fe(II), thereby generating ROS continuously contributing to the enhanced cell death.

On the other hand, extracellular ascorbate oxidation by Fe(III) generates dehydroascorbic acid (DHA), which can be taken up by the cell and reduced back to ascorbate by reacting with a reduced GSH.[66] Ascorbate and reduced GSH can be further consumed by the mIONP-PL-Pt(IV) to generate the cisplatin drugs with GSH exhausting effects providing decreased likelihood of thiol-mediated cisplatin detoxification, which is an important mechanism of cisplatin drug resistance. The role of NADPH oxidase

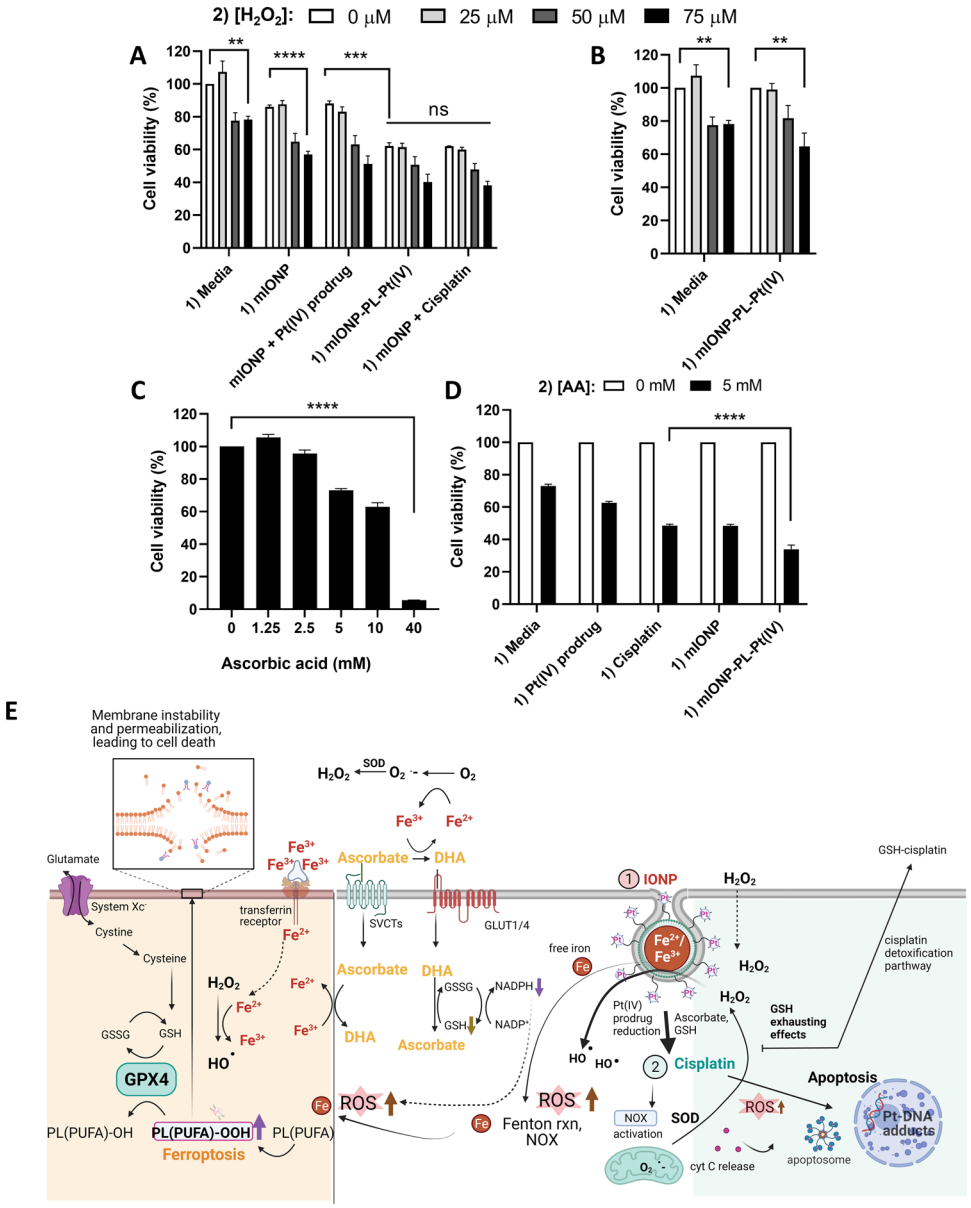

Figure 3. Integrated effects and reactions of H_2O_2, ascorbic acid (AA) and mIONP-PL-Pt(IV) in melanoma cells. A) B16-F10 cell viability study after 24 h treatment with H_2O_2 without and with pre-treatment with iron and platinum-based drugs ([Fe] = 500 μM, [Pt] = 10 μM). B) Cell viability normalized to the group without H_2O_2 treatment. Data (A,B) shown as mean ± SEM (n = 3). C) Cell viability with AA treatment without iron and platinum drug treatment. D) With iron and platinum pre-treatments for 24 h. Excess AA was removed after 1 h treatment, and cells were incubated for an additional 24 h before assessing cell viability. Data (C,D) are means ± SD. *$p < 0.05$, **$p < 0.01$, ****$p < 0.0001$, ns = non-significant by A,B,D) two-way ANOVA and C) one-way ANOVA followed by Tukey's test. Cell viability was assayed by MTT assay. E) Integrated effects showing the mechanisms of action of functional elements and of cancer cell cytotoxicity, and the chemical reactions and catalysis promoted by functional elements and drugs. Created with BioRender.com.

in cisplatin-induced ROS generation in cisplatin-induced cancer cell death has also been established.[71] Consumption of the intracellular reducing potential of GSH and NADPH paired with production of ROS through redox iron chemistry leads to lipid peroxidation of polyunsaturated fatty acids, cell damage, and ferroptosis.

The malignant melanoma cells can be expected to be more susceptible than normal cells to these mechanisms of cell death, enabled or sensitized by the mIONP-PL-Pt(IV) treatment. Cancer cells, due to high demand for easily accessible labile Fe(II) for their survival and growth, upregulate several iron-intake pathways or downregulate iron export and storage pathways, and therefore can be more effectively targeted by the mIONP-PL-Pt(IV). In addition, tumor associated macrophages (TAMs) have been proposed as additional sources of iron,[72,73] and have been shown to act as slow-release reservoirs of nano-therapeutic Pt(IV) pro-drugs.[74] With the administration of pharmacological ascorbate, mIONP-PL-Pt(IV) can also capitalize on other distinct

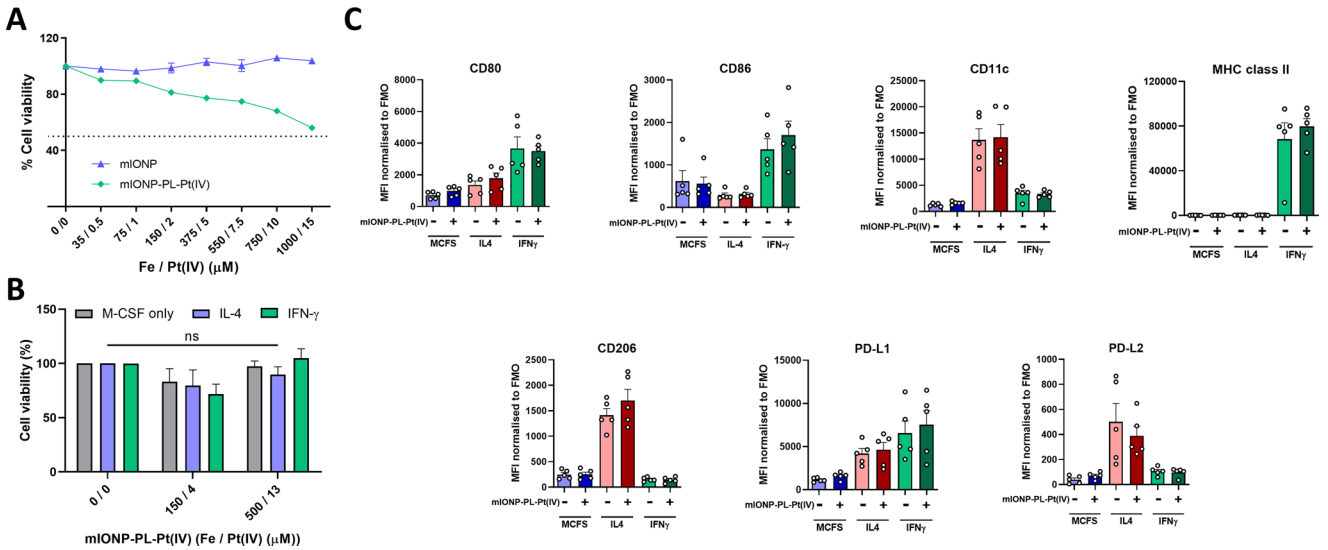

Figure 4. mIONP-PL-Pt(IV) effects on macrophage cell viability and polarization. A) Cell viability of M0 macrophages (RAW264.7) after 24 h treatment with mIONP and mIONP-PL-Pt(IV). B,C) Bone marrow-derived M0 (M-CSF alone), M1 (+IFN-γ), and M2 (+IL-4)-polarized macrophages were exposed to a non-lethal dose of mIONP-PL-Pt(IV) ([Fe] = 150 and 500 μM; [Pt] = 4 and 13 μM) for 24 h and then viability was assessed using an B) MTT assay and polarization markers (CD80, CD86, CD11c, MHC-II, CD206, PD-L1, and PD-L2) were assessed using C) flow cytometry in the presence or absence of mIONP-PL-Pt(IV). Data shown as average mean ± SEM ($n > 4$); ns = non-significant by B) two-way ANOVA and C) one-way ANOVA followed by Tukey's test.

vulnerabilities in cancer such as redox imbalance,[75] and increased DHA uptake via overexpression of glucose transporter 1 (GLUT1) to selectively kill tumor cells.[76]

It is evident from these results that the combined effects of the mIONP and Pt(IV) prodrug delivery result in a combination of redox-triggered effects that enhance melanoma cell death. Notably, in these conventional 2D single cell cultures, which poorly imitate the conditions in vivo, mIONP-PL-Pt(IV) is as potent, but not significantly better, than the co-administration of mIONP and cisplatin. However, mIONP-PL-Pt(IV) was significantly more potent than co-administration of mIONP and Pt(IV) prodrug, which shows that cellular uptake is less effective but more important for the Pt(IV) prodrug than for cisplatin.

2.4. Effects on Macrophage Viability and Polarization

TAMs account for a large proportion of the stromal infiltrate in tumors, and are polarized to a predominantly M2-like immune suppressive anti-inflammatory phenotype.[77] These TAMs also exert a pivotal influence on tumor progression and metastasis and can promote resistance to chemotherapeutic drugs.[78] Thus, induction of cytotoxic effects on the pro-tumoral M2-polarised TAMs could be important to improve the therapeutic efficiency of administered drugs and maximize the outcome of antitumor therapies.[79] Therapeutic effects can also be achieved by reprogramming TAMs from the M2 phenotype toward the antitumoral M1 phenotype.[80,81] On the other hand, the ability of macrophages to sense chemotactic cues and home to tumors with high efficiency, combined with their phagocytic capacity, make them appealing as vehicles for cancer drug delivery. Several studies have also established a paradigm for therapeutic NP drug delivery based on the principle that TAMs can sequester the therapeutic NP payload and gradually release it into the surrounding tissue, thereby serving as "drug depots."[74,82,83] However, the drug delivery role of macrophages requires attaining a high drug loading without compromising macrophage cell viability and functions. Hence, we studied the effects of mIONP-PL-Pt(IV) on macrophage viability and repolarization as well as for potential selectivity of the cytotoxic effects on M1- and M2-polarized macrophages.

To explore the cytotoxicity, RAW 264.7 macrophages were incubated with mIONPs or mIONP-PL-Pt(IV) for 24 h and the cell viability was determined by MTT assay. As expected, the mIONP-PL-Pt(IV) is significantly more cytotoxic to macrophages than mIONPs (**Figure 4**A).

To study the effect of mINOP-PL-Pt(IV) on macrophage repolarization, we exposed mouse bone marrow derived macrophages (BMDMs) to a high dose of mIONPs or mIONP-PL-Pt(IV) (selected from Figure 4A). BMDMs were polarized toward M1-like and M2-like phenotype in the presence of IFN-γ[84] and IL-4, respectively. M0 macrophages did not receive additional stimulation.[85] Stimulation with macrophage colony-stimulating factor (M-CSF) can induce a pseudo M2-like phenotype, that exhibits many of the phenotypic and functional characteristics of TAMs.[86,87] Following mIONP-PL-Pt(IV) treatment, macrophage viability and surface marker expression typical of polarization were analyzed by flow cytometry. No significant macrophage toxicity was observed after treatment with mIONP-PL-Pt(IV) (150 μM or 500 μM [Fe]), with a cell viability above 75% for M1-like and M2-like macrophages (Figure 4B). The analysis of the expression of M1-related surface markers (CD86, CD80, CD11c, and MHCII)[84] and M2-associated expression of CD206 and the immune modulatory receptors (PD-L1– and PD-L2)[88–90] showed no therapy-mediated re-polarization of macrophages (Figure 4C). The lack of significant differences in the expression levels of

surface markers analyzed suggests that mIONP-PL-Pt(IV) treatments do not have a significant effect on macrophage phenotype at the concentrations tested (Figure 4C). Overall, these results indicate that macrophage cell uptake of mIONP-PL-Pt(IV) could allow macrophages to act as carriers for therapy delivery, but it seems less likely they would potentiate TAM-modulating cancer immunotherapies by depletion of tumor-promoting M2 TAMs or a shift toward tumor-suppressive M1-type macrophages.

2.5. Cytotoxic Effects in Co-Cultures

Macrophages can suppress the effects of anti-cancer therapies[91–93] and, as such, we elected to study whether macrophages may represent a barrier to tumor killing by mIONP-PL-Pt(IV). Hence, we next explored the effects of mIONP-PL-Pt(IV) treatments in a co-culture system in which RAW264.7 macrophage cells were seeded on top of B16-F10 melanoma cells at a ratio of 1:3 to 1:2. Cell viability of each cell type post treatment was evaluated using flow cytometry.

Administration of cisplatin leads to high (10 μM cisplatin dose) to complete (100 μM cisplatin dose) elimination of the macrophage cell population, which in turn appears to promote melanoma cell proliferation (Figure S5A, Supporting Information). In contrast, the free Pt(IV) prodrug administration did not lead to noticeable effects on melanoma or macrophage cell viability. Only mIONP-PL-Pt(IV) triggered a significant decrease in melanoma cell viability compared to cisplatin ($p = 0.0068$). Unlike in single cell cultures (Figure 3A), in the co-cultures mIONP-PL-Pt(IV) was consistently more toxic in the melanoma cells than the co-administration of mIONP + cisplatin, albeit not to a significant extent (Figure S5A, Supporting Information). To explore the potential role of ferroptosis in the cell death mechanism and selectivity, lipid peroxidation was probed by Liperfluo and analyzed by flow cytometry. The assays confirmed higher lipid hydroperoxide accumulation in melanoma cells than in macrophages after the treatments and showed that the Pt(IV) cargo contributes toward enhancing the level of lipid peroxidation (Figure S5B, Supporting Information). These results are consistent with recent studies showing that unlike cancer cells, macrophages are quite resistant to oxidative damage and ferroptosis,[94] and the ability of cisplatin to disrupt cellular antioxidant capacity and induce ferroptosis. Overall, these studies support the potential offered by mIONP-PL-Pt(IV) as anti-cancer-selective oxidative stress-inducing therapy that is integrated in the Pt(IV) prodrug nanoparticle delivery approach.

2.6. Bio-Distribution of mIONP-PL-Pt(IV) Demonstrates Accumulation within the Tumor and LNs

Tumor-draining LNs and lymphatic vessels actively facilitate tumor cell dissemination.[14,95,96] Lymph fluid and lymphatic trafficking provide the spontaneously metastasizing melanoma cells with an enhanced ability to withstand oxidative stress and gain protection from ferroptosis.[41] Further relevance for targeting oxidative stress inducing drugs and ferroptosis agents to LNs and lymphatic vessels comes from recent studies showing that multistage differentiation defines melanoma subtypes that are resistant to current treatment options[97] and have enhanced vulnerability to ferroptosis.[98]

To investigate the potential to deliver the mIONP-PL-Pt(IV) treatment to tumor and lymphatic tissues, we ^{67}Ga-radiolabeled the IONP surface exploiting the similarity between Ga(III) and Fe(III) as reported previously.[49] We assessed the stability of the ^{67}Ga-doped mIONP-PL-Pt(IV) by quantifying ^{67}Ga release in PBS at 37 °C. The studies showed good stability, with less than 10% of the bound ^{67}Ga being released over 24 h. The similar radiolabeling stability found in the presence of a large excess of DOTA chelator confirmed that the nanoparticles were stable when challenged, and therefore suitable for in vivo tracking of the IONP-PL-Pt(IV) system (**Figure 5**A,B).

For SPECT/CT imaging we implanted B16–F10 melanoma cells in the left flank of syngeneic C57BL/6 mice, and after tumor establishment, and ^{67}Ga-doped mIONP-PL-Pt(IV) were injected in the peritumoral region or in the hock. The results show that even the mIONP-PL-Pt(IV) administered into the hock (i.e., far from the tumor implantation site) selectively accumulates in LNs and tumor (Figure 5C–F). This biodistribution is also consistent and confirms the lymphatic drainage from the tumor implantation site (hock administration Figure 5C–F, peritumoral administration Figure S6A–C, Supporting Information). Particles clear from the injection site and accumulate at the TDLNs after 3, 24, and 48 h post-injection. IONP-PL-Pt(IV) residing at LNs distant from the injection site is also seen. The results demonstrate that mIONP-PL-Pt(IV) are quickly taken up into lymphatic vessels and transit to the draining LN after injection and/or by the lymphatic migration of the therapy loaded immune cells upon mIONP-PL-Pt(IV) administration. Peritumoral lymphatics are responsible for providing an access route and ferroptosis resistance to cancer cells during metastasis. Here, the IONP-PL-Pt(IV) system is able to use the peritumoral lymphatics to target the tumor tissue and TDLN without direct intratumoral injection.

2.7. In Vivo Inhibition of Tumor Growth

To evaluate whether Pt(IV) delivery by mIONP is beneficial compared to the administration of cisplatin and mIONP alone or combined with mIONP, we implanted a highly immunogenic ovalbumin (OVA) expressing B16-F10 cell line (3×10^5 cells) with or without co-administration of free cisplatin, Pt(IV) prodrug, mIONP, mIONP-PL-Pt(IV) and mIONP + cisplatin (0.55 mg Pt kg^{-1}; 10 mg Fe kg^{-1}). To quantify the relative importance of the mIONP stealth hydrophobic portions, which can provide immune activation[44,47] and improve tumor accumulation,[99] compared to the IONP core alone, one of the groups was treated with the same dose of FDA-approved iron supplement fexumoxytol, where similar IONPs are coated with carboxymethyl dextran. We found that mIONP-PL-Pt(IV) significantly suppressed tumor growth compared to mIONP (100% at 20 days post-inoculation; $p = 0.0058$) with no detectable tumor masses up to 24 days, whereas mice treated with free Pt(IV) prodrug all succumbed to tumors with no survival benefits relative to the saline control group (**Figure 6**). In agreement with our previous studies, some tumor growth inhibition was achieved with mIONP.[45] In contrast, with ferumoxytol, tumor growth was indistinguishable to mice receiving no treatment, which confirms the aggressive

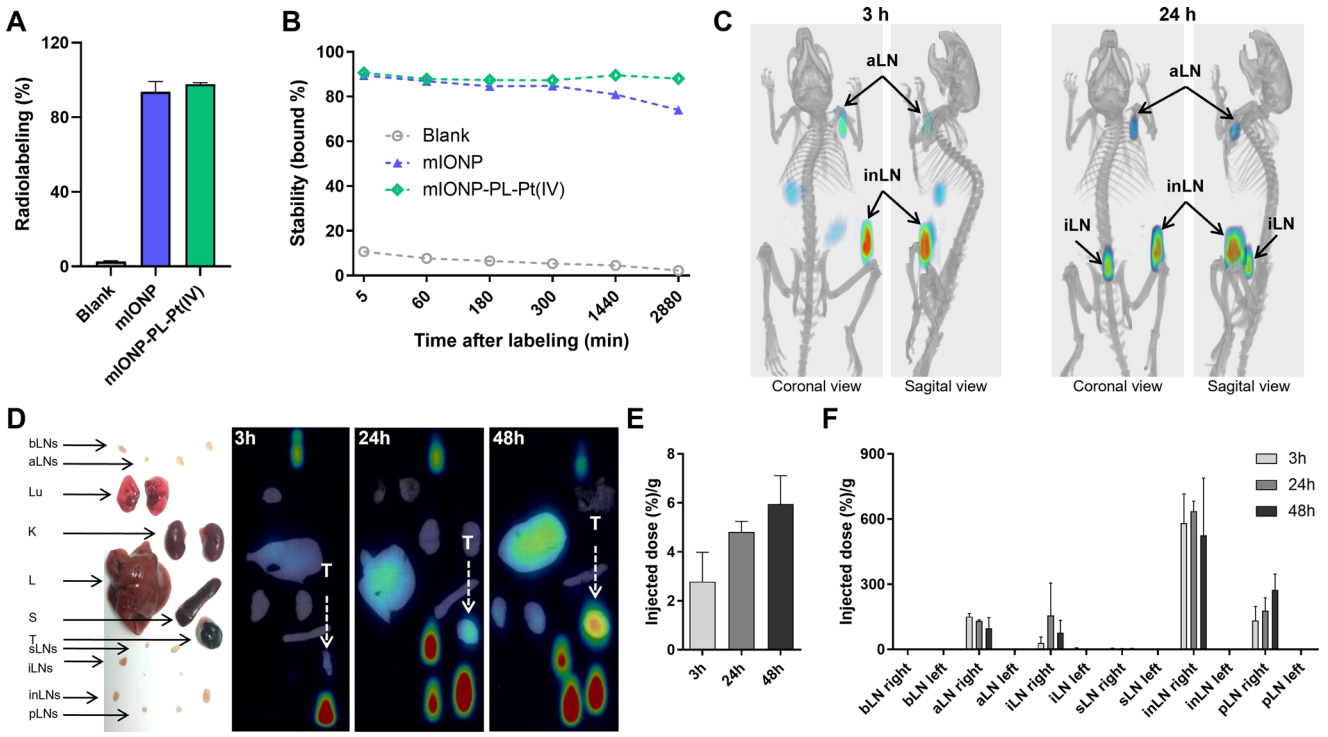

Figure 5. Subcutaneous administration of mIONP-PL-Pt(IV) showed excellent lymphatic drainage and targeting of tumor and lymph nodes. A) ^{67}Ga radiolabeling efficiency). B) Stability over the time of after incubation with > 10^6-fold molar excess of the chelator DOTA. C–F) Biodistribution studies of mIONP-PL-Pt(IV) in tumor bearing mice injected subcutaneously in the right hind hock ([Fe] = 3 mM, 23 MBq). C) In vivo SPECT/CT images at 3 and 24 h after the injection. D–F) Ex vivo analysis of the biodistribution after 3, 24, and 48 h. D) Photograph and SPECT/CT image of selected harvested organs. E) mIONP-PL-Pt(IV) accumulation in the tumor over the time (injected dose percentage per gram of tissue). F) Biodistribution expressed as injected dose percentage per LN. Data are presented as mean ± SEM of two mice. T, tumor; bLN, brachial LN; aLN, axillary LN; Lu, lungs; L, liver; S, spleen; K, kidneys; iLN, iliac LN; sLN, sciatic LN; inLN, inguinal LN; pLN, popliteal LN, injection site (I).

and difficult to treat nature of this tumor model. Treatment with mIONP-PL-Pt(IV) led to delayed tumor growth and prolonged survival compared to cisplatin and IONP. Importantly, under in vivo conditions mIONP-PL-Pt(IV) was also more effective than co-administration of mIONP and cisplatin, clearly demonstrating the importance of the nanoparticle-mediated lymphatic trafficking.

To further assess the therapeutic efficacy of IONP-PL-Pt(IV), C57BL/6 mice were inoculated subcutaneously with 3×10^5 B16-F10(OVA) cells and once they developed an established tumor, they were treated with small doses of mIONP-PL-Pt(IV), cisplatin or Pt(IV) prodrug (0.24 mg Pt kg^{-1}; 5 mg Fe kg^{-1}) on days 7, 10, and 13. Moreover, we also explored transforming growth factor-β (TGF-β) signaling inhibition as a strategy to improve anticancer potential and nanoparticle tumor penetration capacity of therapeutic nanoparticles.[100,101] The release of TGF-β into the TME prevents from the induction of proper anti-tumor immune responses.[102] Here, mice were intraperitoneally injected with the TGF-β inhibitor (TGF-β-I, LY364947) (1 mg kg^{-1}) at 1 h before peritumoral administration of mIONP-PL-Pt(IV), cisplatin or Pt(IV) prodrug. When comparing all treatment groups, the most striking and significant reduction in tumor growth rate was observed in the mice receiving LY364947 and mIONP-PL-Pt(IV) (**Figure 7**A,D).

Tumor size in treated and untreated mice correlated with their survival. Administration of Pt(IV) prodrug did not improve survival over untreated controls, whereas cisplatin increased average survival times (Figure 7B). The mIONP-delivered combination of Pt(IV) prodrug, pro-oxidation, and "stealth" hydrophobicity dramatically increased survival (Figure 7B). Administration of Pt(IV) prodrug-free mIONP also improved survival and showed markedly smaller tumors and longer survival compared to the treatment groups without IONPs, but to a lesser extent than mIONP-PL-Pt(IV). Of the animals receiving LY364947 + mIONP-PL-Pt(IV), 60% survived through the study endpoint at 45 days after initial tumor implantation. No loss of body weight was observed in any group, which suggests the treatments are well-tolerated (Figure 7C).

These results demonstrate the efficacy of the mIONP-PL-Pt(IV) system. In cisplatin protocols in tumor-bearing mice, cisplatin dosing varies from 1–40 mg kg^{-1} as a single or in repeated (multiple) administrations (typically 3–10 over 1–3 weeks).[103] In nanoparticle formulations used in novel combination therapy approaches, cisplatin and Pt(IV) prodrugs platinum doses range from 0.65 to 1.2 mg kg^{-1} for intratumorally administration[104,105] and 1–6 mg kg^{-1} intravenously or intraperitoneally administrations, with cumulative platinum doses of 7.5–20 mg kg^{-1}.[106,107] In our studies, the cumulative platinum dose was <0.75 mg kg^{-1}, which is quite significant considering also that the B16-F10 melanoma model is a very aggressive tumor. This cumulative platinum-drug dose is more than two orders of magnitude lower than the allometric doses used in the clinic for platinum,[108,109]

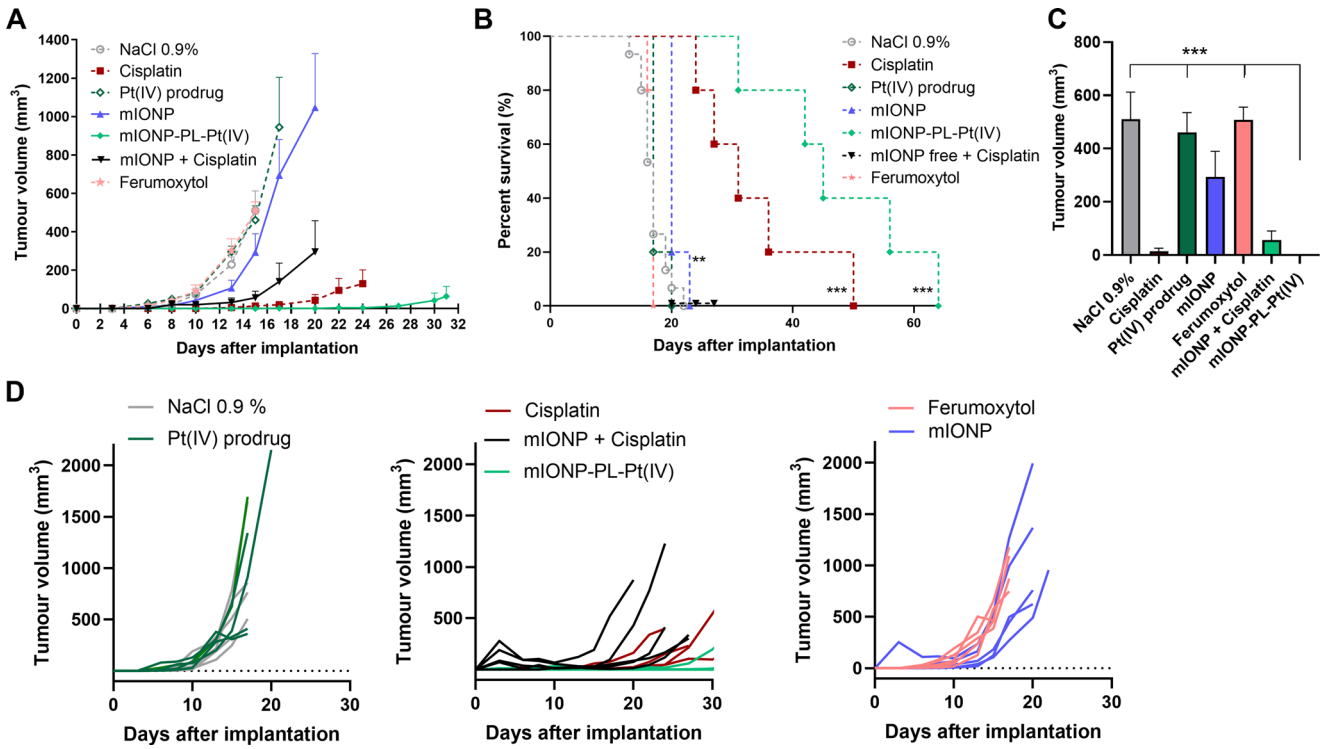

Figure 6. Melanoma tumor growth inhibition with mIONP-PL-Pt(IV) treatment. C57BL/6 mice were implanted 3×10^5 B16-F10(OVA) cells in the right flank with and without platinum and iron nanoparticle treatments (0.55 mg Pt kg^{-1}; 10 mg Fe kg^{-1}). A) mIONP-PL-Pt(IV) inhibited tumor growth more effectively than any other platinum or IONP treatment. B) Survival curves in different treatment groups. C) Tumor volume at day 15. D) Individual tumor growth curves in mice for the different treatment groups. Data are displayed as mean tumor volume of 5 animals per group (**$p < 0.01$, ***$p < 0.001$ by B) log rank (Mantel-Cox) test against NaCl 0.9% group, and C) one-way ANOVA followed by Tukey's test).

which emphasizes the potential of exploiting lymphatic delivery and iron in potentiating and targeting the therapy effect to allow a dose below that which is used in the clinic.

3. Conclusion

In this work, we have studied the redox activation of cytotoxicity, biodistribution, and lymphatic trafficking and therapeutic performance of cisplatin delivered as Pt(IV) prodrug in micelles filled with IONPs in an aggressive and difficult to treat mouse melanoma model. Created by self-assembly of clinically used building blocks, the mIONP-PL-Pt(IV) integrated a number of key functional features, including the iron oxide core, "stealth" hydrophobic segments, and the Pt(IV) center tethered to the phospholipid micelle, while maintaining a particle diameter of between 10 and 100 nm. Each of these design elements imparts benefits and makes the cancer therapy feasible in general issues related to practical and clinical feasibility, including 1) high iron-based catalytic activity that can target ferroptosis in cancer cells and be further enhanced by ubiquitous redox-active H_2O_2 and ascorbate molecules; 2) reduced toxicity relative to the FDA-approved platinum drugs; 3) possibility of multimodal imaging and multimodal therapy combination; and 4) ability to provide effective lymphatic trafficking and delivery of the therapy with a simple, yet multifunctional nanoformulation.

The mIONP-PL-Pt(IV) was designed and tested for delivery and release of cisplatin with simultaneous Fe(II)/Fe(III)-induced cytotoxic effects triggered by ROS, Fenton reaction, and peroxidase-like activity. The in vitro studies showed high peroxidase-like activity, and in melanoma cells the cytotoxicity was as potent as with cisplatin, inducing greater lipid peroxidation and significantly enhanced cytotoxic effects in the presence of both H_2O_2 and ascorbic acid. The scope for macrophage-mediated cancer therapy and drug delivery was also studied. Although macrophages cannot be ruled out as playing a role in vivo acting as carriers of mIONP-PL-Pt(IV), it is less likely they would undergo phenotypic/functional switch. Indeed, potentially as important as the chemical reactivity provided by this bioinorganic nanoformulation, mIONP-PL-Pt(IV) was designed and tested for targeting lymphatic delivery of the therapy. The ^{67}Ga-radiolabeled mIONP-PL-Pt(IV) was found to effectively transit to the draining LNs and tumor from distant subcutaneous injection sites, as well as the ability to use the peritumoral lymphatics to target the tumor tissue and TDLN without direct intratumoral injection. This provided the opportunity of delivering the iron and platinum therapy to tackle the problem of cancer cell lymphatic migration, which has been recently shown to facilitate resistance and protection from similar cancer treatments and from ferroptotic cell death, which is emerging as an orthogonal therapeutic approach to target the differentiation plasticity of melanoma cells to increase the efficacy of targeted and immune therapies. In therapy studies, subcutaneously administered mIONP-PL-Pt(IV) provided significant melanoma tumor inhibition at low doses (cumulative Pt and Fe dose <1 mg kg^{-1} and <15 mg kg^{-1} of

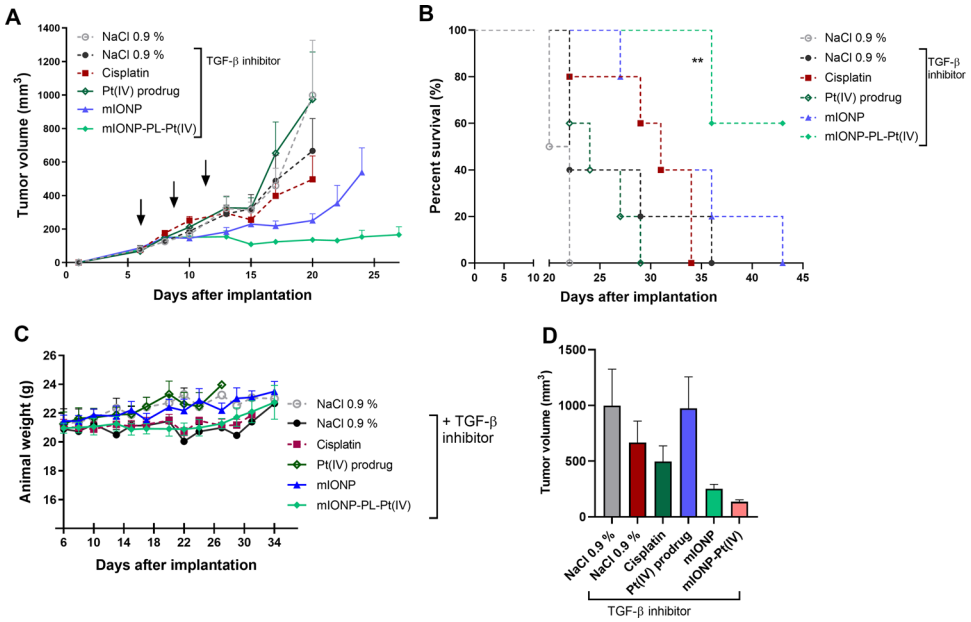

Figure 7. Therapy in established melanoma tumors. C57BL/6 mice were implanted 3×10^5 B16-F10(OVA) cells in the right flank and once tumor was established, they were administered by hock s.c. injection of small treatment doses on days 7, 10, and 13 (0.24 mg Pt kg^{-1}; 5 mg Fe kg^{-1}, $n = 5$ mice for each group). In each treatment group LY364947 was administered by i.p. injection 1 h prior to the treatments. A) Tumor growth inhibition; mIONP-PL-Pt(IV) is more effective than any other platinum or IONP treatment. B) Survival results (Kaplan–Meier) of tumor therapy with mIONP-PL-Pt(IV) treatment compared with control group and other iron oxide and platinum-based treatments. Asterisks indicate $^{**}p < 0.01$ for mIONP-PL-Pt(IV) group compared with control group (NaCl 0.9% + TGF-β inhibitor) by log rank (Mantel-Cox) test. C) Body weight variation of treated mice following the s.c. administrations of the different treatments. D) Tumor volume at day 20; $^{*}p < 0.05$ by unpaired *t*-test). Mean values and error bars are defined as mean and ± SEM.

body weight, respectively) without apparent toxicity and, improving treatment compared to free cisplatin or co-administration of mIONP + cisplatin. It is worth underlying that we expect these and related systems to be applicable for lymphatic delivery of the therapy and result in therapeutic improvements in other tumor models. Furthermore, there is major scope for optimizing and customizing the IONP, Pt(IV) prodrug, and coating ligands and use in combination with other drugs/therapy, with an already experimental basis for exploring the synergistic action of platinum-based therapy as nanoformulations in immunotherapy.

4. Experimental Section

Materials: All syntheses were carried out with the following commercially available reagents used without further purification. Chloroform (water 0.005%) and hexane (99%) were purchased from LABSCAN, dimethylsulfoxide (≥99.5%) was purchased from Panreac. LABSCAN), diphenyl ether (99%), oleylamine (70%), 4-(dimethylamino)pyridine (99%), *N,N′*-dicyclohexylcarbodiimide (99%) and LY364947 were purchased from Sigma Aldrich, dibenzyl ether (>98%) and oleic acid (90%) were purchased from Alfa Aesar, 1,2-hexadecanediol (>98%) from Tokyo Chemical Industry Co. Ltd), iron(III) acetylacetonate (99%) from Strem Chemicals and ethanol (99%+) from Fisher Chemical).1,2-Dipalmitoyl-*sn*-glycero-3-phosphoethanolamine-N-[methoxy(polyethylene glycol)-2000] (ammonium salt) (DPPE-PEG(2000)), 1,2-distearoyl-sn-glycero-3-phosphoethanolamine-N-[carboxy(polyethylene glycol)-2000] (ammonium salt) (DSPE-PEG(2000)-COOH), 1,2-distearoyl-*sn*-glycero-3-phosphoethanolamine-N-[amino(polyethylene glycol)-2000] (ammonium salt) (DSPE-PEG(2000)-NH_2) and 1,2-dipalmitoyl-*sn*-glycero-3-phosphoethanolamine-N-(lissaminerhodamine B sulfonyl) (Rho-PE) were purchased from Avanti Polar Lipids. *cis,trans*-$[Pt(NH_3)_2Cl_2(O_2CCH_2CH_2CO_2H)_2]$ and hydrophobic IONPs were prepared according to previously reported methods.[110,111]

Synthesis of DSPE–PEG(2000)–Pt(IV): In a typical reaction, *cis,cis,trans*-$[Pt(NH_3)_2Cl_2(O_2CCH_2CH_2CO_2H)_2]$ (9.6 mg, 18.0 µmol), dicyclohexylcarbodiimide (DCC) (3.7 mg, 18.0 µmol) and 4-(dimethylamino)pyridine (1.0 mg, 7.2 µmol) were dissolved in DMSO (130 µL).[58] This solution containing the activated platinum (IV) complex was added to a DMSO solution of DSPE-PEG(2000)-NH_2 (10 mg, 3.6 µmol, 170 µL). The resulting mixture was allowed to react at room temperature for 72 h under continuous stirring. Water was then added to the reaction mixture and the solution was centrifuged to remove the insoluble material. The supernatant was filtered (0.45 µm) and dialyzed in a Slide-A-Lyzer dialysis cassette (Thermo Scientific) (MW cut-off 2000 Da) against water. The dialyzed product was characterized by ^{1}H NMR and UPLC-ESI-MS/MS (Figures S1 and S2, Supporting Information), lyophilized, and stored for use in the next experiments.

Preparation of mIONP and mIONP-PL-Pt(IV): For the preparation of the IONP-filled micelles hydrophobic Fe_3O_4 nanoparticles (0.5 mg) and DSPE-PEG(2000)-COOH or DPPE-PEG(2000) (100 µL of a 10 mg mL^{-1} solution in $CHCl_3$ for preparing control micelles) or DSPE-PL-Pt(IV) (100 µL of a 10 mg mL^{-1} solution in 1:2 MeOH:$CHCl_3$ for platinum-loaded micelles) were dissolved in $CHCl_3$ (500 µL).[112] Fluorescent micelles were prepared by introducing a commercial rhodamine labeled phospholipid into the mixture (15 µL from a 2 mg mL^{-1} solution). The solvent was allowed to evaporate overnight at room temperature. Any remaining solvent was removed under vacuum. The dried residue was heated in a water bath at 80 °C for 30 s, after which 1 mL of nanopure Milli-Q water was added. To maximize the yield of product formation, mIONPs were left to hydrate at room temperature for 2 h. Large aggregates were removed by centrifugation (1 cycle, 9800 × *g*, 5 min) and the supernatant was passed through a 0.45 µm PTFE syringe-filter. Any remaining empty micelles were removed by ultracentrifugation (3 cycles, 160 000 × *g*, 50 min) by discarding the supernatant.

Quantitation of Platinum and Iron Loading: Platinum loading in the mIONP-PL-Pt(IV) samples was quantified combining a UV–vis spectrophotometric method[56] and inductively coupled plasma atomic emission spectroscopy (ICP-AES). The colorimetric assay was based on the substitution of the labile cis-chloride ligands in Pt(II)-complexes by orthophenylenediamine (OPD) to yield Pt(II)-OPD compounds showing a strong absorbance peak at 706 nm. For this assay an aliquot of a Pt-containing sample was dissolved in 100 µL of DMF and added to 50 µL of PBS and 500 µL of a fresh solution of 10 mg mL^{-1} of OPD in DMF. The reaction mixture was left to react for at least 12 h at 80 °C under continuous stirring. After cooling to room temperature, the amount of Pt present in the sample was determined by measuring the absorbance at 706 nm and using Lambert–Beer's law and calibration curves obtained for known increasing amounts of the Pt(II) and Pt(IV) compounds ([Pt] = 0–10 µM). The platinum colorimetric quantification was calibrated and validated with ICP-AES. The concentration of iron in the mIONP solutions was estimated by UV–vis from the absorbance at 380 nm using calibration curves obtained using mIONPs samples for which the iron content had been determined by ICP-AES.

mIONP Peroxidase-Like Catalytic Activity Studies: The peroxidase-like activity of the mIONPs was studied by monitoring the oxidation of TMB by UV–Vis spectroscopy, which yields a blue product (λ = 652 nm) product. The Michaelis-Menten kinetics assays were conducted with IONP-containing formulations at the indicated concentrations in sodium acetate buffer (pH = 4.5) and TMB (830 µM) in the presence of different concentrations of H_2O_2 (ranging from 0.060 to 30.3 mM) The kinetic parameters were calculated fitting the absorbance data using Lineweaver–Burk plots of the Michaelis–Menten kinetics using GraphPad Prism 6.02 (GraphPad Software).

$$\frac{1}{\nu} = \frac{Km}{V\max}\left(\frac{1}{[S]} + \frac{1}{Km}\right) \quad (1)$$

where ν is the initial velocity, Vmax is the maximal reaction velocity, [S] is the concentration of substrate and Km is the Michaelis constant and the turnover number (k_{cat}) was calculated as,

$$k_{cat} = \frac{V\max}{[E]} \quad (2)$$

where [E] stands for enzyme concentration, in this work the iron oxide nanozyme concentration [IONP], which was estimated from the iron concentration and IONP size as described previously.[45]

Cell Uptake and Viability Experiments: The B16-F10 melanoma cells were purchased from the American Type Culture Collection (ATCC) and the isogenic B16-F10(OVA) cells were obtained as a gift from Dr. Pablo Sarobe (Centre for Applied Medical Research (CIMA), University of Navarra)). Cells were cultured in RMPI 1640 (Lonza) supplemented with 10% fetal bovine serum (FBS), 1% penicillin/streptomycin, and L-Glutamine (all from Glibco) and maintained in a humidified atmosphere of 5% CO_2 at 37 °C.

Cytotoxicity Studies: The cells were seeded (1×10^4 cells $well^{-1}$ in complete RPMI 1640 medium) in 96-well plates (100 µL $well^{-1}$) and cultured for 24 h. Then, the samples to be tested were accordingly diluted in media and added directly to the cells (100 µL $well^{-1}$), with a minimum of three replicates. After incubation with the treatments at 37 °C, cell viability was measured using MTT assay. Briefly, 50 µL $well^{-1}$ of MTT reagent (0.5 mg mL^{-1} in RPMI 1640) was added after the removal of the supernatants. Cells were incubated at 37 °C for 2 h after which the media was removed and the lysis solution added (DMSO, 100 µL $well^{-1}$). The absorbance was measured using a POLARstar Omega (BMG Labtech) microplate reader at 550 nm to determine the relative cell viability.

Cellular Uptake and Distribution Studies: The B16-F10 melanoma cells were plated in an ibidi 15 well angiogenesis µ-Slide at a density of 4×10^4 cells $well^{-1}$ and allowed to adhere overnight in the presence of complete RPMI 1640 medium. Then, the medium was removed and fresh medium containing the rhodamine labeled Pt-loaded mIONP was added and incubated for 2 h. Nuclei were stained with Hoechst 33342 (1 µg mL^{-1} in RPMI 1640 medium) for 5 min. After nuclei staining the cells were washed twice with PBS (10 mM) and fresh medium was added. A Zeiss Axio Observer wide field fluorescence microscope (Carl Zeiss, Germany) was used to visualize the cells. Brightfield and fluorescence images were collected and processed using AxioVision and ZEN software.

Macrophage Polarization and Viability Studies: Murine BMDMs were generated for experiments by flushing BM from the femur and tibia of FVB/NCrl mice using a syringe and needle. RBCs were lysed using RBC lysis buffer (Roche). Cells were numerated using trypan blue exclusion and plated in RPMI 1640, 10% FCS, 1% penicillin/streptomycin (Sigma Aldrich), 10 ng mL^{-1} recombinant murine M-CSF (Bio-Techne) at 5×10^5 cells $well^{-1}$ on 12 well plates for 72 h prior to subsequent downstream analyses. Where M1/M2 macrophages phenotypes were required, additional murine polarizing cytokines, IL-4 (M2) or IFN-γ (M1) (Bio-Techne) were added at 50 ng mL^{-1} at 48 h post plating when macrophages had differentiated. Wells were then washed and replaced with fresh media prior to exposure to nanoparticles. Cell viability was assessed in the wells using a MTT assay as described above. This time instead, cells were incubated at 37 °C for 3–4 h after which the media was removed, and the converted dye was solubilized with acidified isopropanol (0.04 N HCl in absolute isopropanol). For characterizing the phenotype of macrophages after 24 h of exposure to the nanoparticles, cells were recovered from the well using enzyme-free cell dissociation buffer (Thermo Fisher Scientific) prior to staining for flow cytometry analyses.

Cell Monocultures: The B16 melanoma cells were plated in 96-well plates (1×10^5 cells $well^{-1}$) and allowed to adhere overnight in complete RMPI 1640 medium. Fluorescent formulations containing rhodamine labeler Pt-loaded mIONP were diluted in medium accordingly and added to the cells at a final concentration of 1 mM Fe for 2 h incubation at 37 °C. After the incubation, the supernatant was removed, and cells washed with PBS. The adherent cells were transferred to cytometer tubes and washed with PBS (10 mM). Cells were resuspended in a final volume of 200 µL of flow cytometry buffer (1% BSA, 0.1% sodium azide in PBS 10 mM). Rhodamine uptake was measured using a FACS Canto II (BD Biosciences) and the data were analyzed using the FlowJo, LLC software. Cells were electronically gated based on forward and side scatter parameters and the not-singlet events were left out based on forward area and height scatter parameters. The laser excitation wavelength used for rhodamine was 488 nm and the emission filter 585/21 nm. Each analysis represented the acquisition of 1×10^5 cells per sample.

Flow cytometry with the murine BMDMs was performed as previously described.[113] Fc receptors were blocked using anti-mouse CD16/32 (2.4G2; Tonbo Biosciences) for 30 min prior to staining. The following antibodies against the indicated antigen were purchased from Thermo Fisher Scientific and were used at 1 µg mL^{-1} unless stated otherwise: CD11c FITC (N418; Biolegend), CD206 FITC (C068C2; Biolegend), F4/80 APC-eFluor 780 (BM8), MHCII BV421 (M5/114.15.2), PD-L1 PE (MIH5), PDL-2 APC (TY25; Biolegend), CD80 APC (16-10A1) and CD86 PE (GL-1; Biolegend). Positive stains were compared to fluorescence minus one (FMO) controls. Dead cells were excluded using 1 µg mL^{-1} 7-amino actinomycin D (7AAD; Sigma Aldrich). Data were collected on a BD FACS Canto II (BD Biosciences). Data were analyzed using FlowJo software (BD biosciences).

Contacting Cell Co-Cultures: The contacting cell co-culture was developed to obtain a homogeneous monolayer of B16 cells obtaining a macrophage-to-melanoma cell ratio of ≈1:3 to 1:2, which corresponds to the relative macrophage-to-cancer cell presence observed in human tumors.[114,115]

B16-F10 melanoma cells were seeded in 96-well plates at a density of 5.8×10^4 cells in a volume of 200 µL. After 24 h, B16-F10 cells formed a confluent monolayer and 8.5×10^4 RAW264.7 macrophage cells were seeded on top (seeding density of 2.7×10^5 cells cm^{-2}) in a volume of 100 µL. They were allowed to adhere for 2 h in complete medium (media mix ratio of RPMI 1640:DMEM = 7:1). Medium was removed and fresh RPMI 1640 medium was added for 30 min to stabilize the cells. Finally, medium was removed, and treatment was added as specified. Every treatment was performed in triplicate. Cells were detached using 100 µL accutase trypsin and neutralized after a 5-min incubation at room temperature with 100 µL of complete RPMI 1640 medium. Detached cell populations

were pooled together for subsequent Flow Cytometry experiments. The cell suspensions were washed with PBS by centrifugation (2 cycles, 800 × *g*, 4 min). The cell suspensions were washed with PBS by centrifugation (2 cycles, 800 g, 4 min) and stained with 50 µL of Zombie NIR diluted 1:100 in PBS over 45 min at 4 °C in the dark. For differentiation between RAW from B16, cells were then washed with 0.1% BSA in PBS and stained with Brilliant Violet-labeled anti-F4/80 antibody diluted 1:200 in the same buffer. Finally, the cell suspensions were washed with FACS buffer (1% FBS in PBS) by centrifugation (2 cycles, 800 g, 4 min) and suspended in 300 µL of the same buffer. Positive controls for necrotic cell death were heated to 80 °C for 3 min prior to staining. Using a NovoCyte Flow Cytometer (ACEA Biosciences), cell populations were gated based on the forward and side scatter parameters and the not-single events were left out based on forward area and height scatter parameters (FlowJo, LCC software). Differentiation between cells was based on F4/80-positive fluorescent (fluorescent Pacific Blue channel, 445 nm). Necrotic cell populations were gated based on Zombie NIR positive fluorescent staining (fluorescent APC-Cy7 channel, 780 nm)

Membrane Lipid Peroxidation Analysis in Live Cells: Lipid hydroperoxide accumulation was probed by Liperfluo and analyzed by flow cytometry. The test was performed using Contacting cell co-culture set-ups as described above (when tested on B16-F10 monocultures macrophage addition was omitted). After the treatment, supernatant was removed and cells were stained using Liperfluo (10 µM) or treated with DMSO vehicle control (1%) and incubated 30 min (at 37 °C, 5% CO_2). As a positive control for lipid peroxides, cells were incubated with cumene hydroperoxide (100 µM) in complete RPMI medium for 2 h at 37 °C, 5% CO_2 prior to Liperfluo addition. Cells were detached using 100 µL accutase and prepared for flow cytometry analysis as described above. After not-single events were left out, differentiation between cells was based on lipid hydroperoxide-positive fluorescent staining (fluorescent Pacific Orange channel, 572 nm). Data were analyzed using FlowJo Software.

^{67}Ga-Labeling of the mIONP-PL-Pt(IV): mIONP-PL-Pt(IV) were radiolabeled adopting synthesis-free method as previously described for related nanovaccines.[45,116] In brief, after purification of purchased gallium-67 (^{67}Ga) (Curium, specific activity = 1.4 TBq µmol^{-1}) following a previously reported method,[117] 50 µL of IONPs (≈3 mM of Fe) was mixed with 100 µL of $^{67}GaCl_3$ (≈37 MBq) and diluted up to 500 µL in acetate buffer (pH = 3.8 ± 0.1). Reaction was incubated over 30 min at 70 °C, the reaction crude was cooled down to room temperature, and the labeled IONPs and unbound gallium-67 was removed by two cycles of ultrafiltration (6708 × *g* for 10 min) through Amicon Ultracel (MWCO = 100 kDa) centrifugal devices (Merck), and washed twice with saline solution, after which the retentate was recovered in PBS (10 mM) ready to be injected. The total radioactivity in the filtrate and retentates was measured in a CRC-25R dose calibrator (Capintec, USA) in order to determine the incorporation efficiency. For stability studies, ^{67}Ga-labeled mIONP-PL-Pt(IV) were incubated in the presence of the chelating agent DOTA (10^6 moles of DOTA per mole of nanoparticle) at 37 °C. At different time points, the samples were filtered to separate the IONPs from the ^{67}Ga complexed to DOTA and the radioactivity in the retentate and filtrate was measured. Depending on the activity, samples were measured using a CRC-25R dose calibrator (Capintec, USA) or a 2470 WIZARD^2 Automatic Gamma Counter (PerkinElmer). The dissociation of ^{67}Ga from the radiolabeled micelles was calculated (expressed in percentage) at each time point as the ratio between the amount of radioactivity on the filter and the starting radioactivity.

In Vivo Biodistribution and Therapy Studies: Animals were cared for and handled in compliance with the Guidelines for Accommodation and Care of Animals (European Convention for the Protection of Vertebrate Animals Used for Experimental and Other Scientific Purposes) and internal guidelines. All animal procedures were performed in accordance with the Spanish policy for animal protection (RD53/2013), which meets the requirements of the European Union Animal Directive (2010/63/EU). They were carried out in authorized (ES200690050402), AAALAC-accredited (Unit # 1612) animal facility, and approved by the Ethical Committee of CIC biomaGUNE (code: AE-biomaGUNE-0614) and by local authorities (Diputación Foral de Guipuzkoa; code: PRO-AE-SS-047). All animals were housed in ventilated cages and fed on a standard diet ad libitum.

Tumor Inoculation: C57BL/6 mice (6–8 weeks old) were used for all in vivo experiments. B16-F10-OVA cells were used for the tumor inoculation and were previously cultured similarly to what was described for the in vitro experiments. Prior to injecting in vivo, cells were tested for mycoplasma using the commercially available MYCOALERT Mycoplasma Detection Kit (Lonza). For tumor inoculation 3×10^5 cell mouse^{-1} were dissolved in Corning Matrigel Basement Membrane Matrix High Concentration diluted in PSB 10 mM (1:4 PBS:Matrigel). All the materials (tips, pipettes, syringes, and storage vials) were kept in ice until use and the cell suspension in Matrigel. The suspension was then loaded in a syringe and 100 µL mouse^{-1} injected subcutaneously in the right back of the animals using a 23G needle. Animals were monitored for tumor growth using an electronic digital caliper 779A series (Starrett) until the tumor size was appropriate to start the therapy or SPECT/CT Imaging (≈100 mm^3, ≈7 days from tumor inoculation).

Biodistribution SPECT/CT Studies: C57BL/6 mice (6–8 weeks old) were injected with ^{67}Ga-mIONP-PL-Pt(IV) micelles in saline solution subcutaneously in the peritumoral region or into the hock (injection ranged from 15 to 25 MBq)). With the mouse under isoflurane anesthesia (1.5–2% in oxygen), whole-body SPECT/CT scans were acquired at 3, 24, and 48 h after the injection using an eXplore speCZT CT scanner and an 8-slit collimator with a field of view of 32 and 78 mm in the transaxial and axial directions, respectively. With the full ring detector, 360° of data were acquired by rotating the collimator 45° (45 steps, 1° per step). Data were collected in an energy acquisition window from 125–150 keV to 84–102 keV and acquisition times from 60 min (80 s per step) to 45 min (60 s per step). The CT acquisition consisted of 220 views were acquired in 0.88° increments around the animal with 16 ms exposure per view. The X-ray tube settings were 70 kV and 32 mA. The SPECT images were reconstructed using the OSEM iterative algorithm (5 and 15 subsets, 3 and 5 iterations) into 128 × 128 × 32 array with a voxel size of 0.4 × 0.4 × 2.46 mm and were not corrected for scatter and attenuation. After each SPECT scan, CT acquisitions were performed to provide anatomical information on each animal. The CT images were reconstructed using a cone beam filtered back-projection Feldkamp algorithm into 437 × 437 × 523 array with a voxel size of 0.2 × 0.2 × 0.2 mm. For the quantification of SPECT images, PMOD image analysis software (PMOD Technologies Ltd, Zurich, Switzerland) was employed. During image acquisition, mice were kept normothermic by the use of a heating blanket (Homeothermic Blanket Control Unit; Bruker BioSpin GmbH, Karlsruhe, Germany). At the end of the scanning procedure, the mice were culled by cervical dislocation and organs of interest were removed for further ex vivo SPECT/CT imaging under the same conditions of the in vivo images. Finally, organs were measured using a WIZARD2 2470 Automatic Gamma Counter (PerkinElmer) and the injected dose percentage per organ or per gram of tissue was calculated by normalizing values to the total injected amount of radioactivity.

Tumor Therapy: Therapy was given as a single dose during tumor implantation (Figure 6) or started roughly 1 week after the tumor inoculation (day 0), when the tumor size reached ≈100 mm^3 (Figure 7). In this latter case, the corresponding doses were injected on days 7, 10, and 13 in the subcutaneous peritumoral region (≈2 cm away from the tumor). In each case, 1 h prior to sample administration, TGF-β inhibitor LY364947 (1 mg kg^{-1}) was administered by intraperitoneal injection. The samples were prepared in saline solution (0.9% NaCl) with a fixed concentration of 0.24 mg Pt kg^{-1} for each dose and similar for all the groups (the injected iron concentration never exceeded 5 mg Fe Kg^{-1}). Animals were monitored for tumor growth using an electronic digital caliper 779A series (Starrett). Results of tumor volume, animal weight, and survival rate were expressed as mean ± SEM ($n = 5$).

Supporting Information

Supporting Information is available from the Wiley Online Library or from the author.

Acknowledgements

J.C. and J.C.M.-R. thank an MRC Confidence in Concept award (MC_PC_19053). M.B.-A. was supported by an EPSRC Ph.D. Studentship (project reference 2105067). J.N.A. was funded by a grant from Cancer Research UK (DCRPGF\100009) and is the recipient of a Cancer Research Institute/Wade F.B. Thompson CLIP grant (CRI3645).

Conflict of Interest

The authors declare no conflict of interest.

Author Contributions

M.B.-A., and A.R.-d.-A. contributed to methodology, investigation, formal analysis, and writing—original draft. A.G.A., S.M.-S., and D.S. contributed to investigation. A.Z. contributed to methodology, investigation, formal analysis, and writing—review & editing. J.L. contributed to resources, supervision, and validation. J.N.A. contributed to supervision, resources, validation, funding acquisition, and writing—review & editing. J.C. contributed to supervision, funding acquisition, and writing—review & editing. J.C.M.-R. contributed to conceptualization, methodology, project administration, funding acquisition, supervision, writing—original draft, and review & editing.

Data Availability Statement

The data that support the findings of this study are available in the supplementary material of this article.

Keywords

drug delivery, ferroptosis, iron oxide nanoparticles, lymphatic system, melanoma treatment, platinum(IV) prodrugs, reactive oxygen species

Received: August 8, 2022
Revised: October 15, 2022
Published online:

[1] L. Kelland, *Nat. Rev. Cancer* **2007**, *7*, 573.
[2] S. M. Dadfar, K. Roemhild, N. I. Drude, S. von Stillfried, R. Knüchel, F. Kiessling, T. Lammers, *Adv. Drug Delivery Rev.* **2019**, *138*, 302.
[3] R. A. Revia, M. Zhang, *Mater. Today* **2016**, *19*, 157.
[4] Z. H. Siddik, *Oncogene* **2003**, *22*, 7265.
[5] D. Wang, S. J. Lippard, *Nat. Rev. Drug Discovery* **2005**, *4*, 307.
[6] N. Hanna, L. H. Einhorn, *J. Clin. Oncol.* **2014**, *32*, 3085.
[7] T. C. Johnstone, K. Suntharalingam, S. J. Lippard, *Chem. Rev.* **2016**, *116*, 3436.
[8] P. Ma, H. Xiao, C. Li, Y. Dai, Z. Cheng, Z. Hou, J. Lin, *Mater. Today* **2015**, *18*, 554.
[9] F. Danhier, *J. Controlled Release* **2016**, *244*, 108.
[10] H. He, L. Liu, E. E. Morin, M. Liu, A. Schwendeman, *Acc. Chem. Res.* **2019**, *52*, 2673.
[11] A. Moreira, L. Heinzerling, N. Bhardwaj, P. Friedlander, *Cancers* **2021**, *13*, 221.
[12] H. J. Gogas, J. M. Kirkwood, V. K. Sondak, *Cancer* **2007**, *109*, 455.
[13] S. Vanharanta, J. Massagué, *Cancer Cell* **2013**, *24*, 410.
[14] A. Alitalo, M. Detmar, *Oncogene* **2011**, *31*, 4499.
[15] D. L. Morton, J. F. Thompson, A. J. Cochran, N. Mozzillo, O. E. Nieweg, D. F. Roses, H. J. Hoekstra, C. P. Karakousis, C. A. Puleo, B. J. Coventry, M. Kashani-Sabet, B. M. Smithers, E. Paul, W. G. Kraybill, J. G. McKinnon, H.-J. Wang, R. Elashoff, M. B. Faries, *N. Engl. J. Med.* **2014**, *370*, 599.
[16] E. Piskounova, M. Agathocleous, M. M. Murphy, Z. Hu, S. E. Huddlestun, Z. Zhao, A. M. Leitch, T. M. Johnson, R. J. DeBerardinis, S. J. Morrison, *Nature* **2015**, *527*, 186.
[17] J. L. Martindale, N. J. Holbrook, *J. Cell. Physiol.* **2002**, *192*, 1.
[18] S. Dixon, *Cell* **2012**, *149*, 1060.
[19] X. Jiang, B. R. Stockwell, M. Conrad, *Nat. Rev. Mol. Cell Biol.* **2021**, *22*, 266.
[20] D. P. M. Conrad, *Nat. Chem. Biol.* **2019**, *15*, 1137.
[21] B. Perillo, M. Di Donato, A. Pezone, E. Di Zazzo, P. Giovannelli, G. Galasso, G. Castoria, A. Migliaccio, *Exp. Mol. Med.* **2020**, *52*, 192.
[22] B. Hassannia, P. Vandenabeele, T. Vanden Berghe, *Cancer Cell* **2019**, *35*, 830.
[23] X. Shan, S. Li, B. Sun, Q. Chen, J. Sun, Z. He, C. Luo, *J. Controlled Release* **2020**, *319*, 322.
[24] Z. Shen, J. Song, B. C. Yung, Z. Zhou, A. Wu, X. Chen, *Adv. Mater.* **2018**, *30*, 1704007.
[25] C. Liang, X. Zhang, M. Yang, X. Dong, *Adv. Mater.* **2019**, *31*, 1904197.
[26] M. Huo, L. Wang, Y. Chen, J. Shi, *Nat. Commun.* **2017**, *8*, 357.
[27] H. Lin, Y. Chen, J. Shi, *Chem. Soc. Rev.* **2018**, *47*, 1938.
[28] S. Li, P. Jiang, F. Jiang, Y. Liu, *Adv. Funct. Mater.* **2021**, *31*, 2100243.
[29] Z. Li, C. Wang, C. Dai, R. Hu, L. Ding, W. Feng, H. Huang, Y. Wang, J. Bai, Y. Chen, *Biomaterials* **2022**, *287*, 121668.
[30] H. Xiang, C. You, W. Liu, D. Wang, Y. Chen, C. Dong, *Biomaterials* **2021**, *277*, 121071.
[31] X. Chen, X. Yin, L. Zhan, J. Zhang, Y. Zhang, Y. Wu, J. Ju, Y. Li, Q. Xue, X. Wang, C. Li, R. L. Reis, Y. Wang, *Adv. Funct. Mater.* **2022**, *32*, 2108603.
[32] R. A. Cairns, I. S. Harris, T. W. Mak, *Nat. Rev. Cancer* **2011**, *11*, 85.
[33] U. E. Martinez-Outschoorn, M. Peiris-Pagés, R. G. Pestell, F. Sotgia, M. P. Lisanti, *Nat. Rev. Clin. Oncol.* **2017**, *14*, 11.
[34] Z. Dong, L. Feng, Y. Chao, Y. Hao, M. Chen, F. Gong, X. Han, R. Zhang, L. Cheng, Z. Liu, *Nano Lett.* **2018**, *19*, 805.
[35] S. Gao, Y. Jin, K. Ge, Z. Li, H. Liu, X. Dai, Y. Zhang, S. Chen, X. Liang, J. Zhang, *Adv. Sci.* **2019**, *6*, 1902137.
[36] W.-P. Li, C.-H. Su, Y.-C. Chang, Y.-J. Lin, C.-S. Yeh, *ACS Nano* **2016**, *10*, 2017.
[37] Z. Zhou, J. Song, R. Tian, Z. Yang, G. Yu, L. Lin, G. Zhang, W. Fan, F. Zhang, G. Niu, L. Nie, X. Chen, *Angew. Chem., Int. Ed.* **2017**, *56*, 6492.
[38] P. Ma, H. Xiao, C. Yu, J. Liu, Z. Cheng, H. Song, X. Zhang, C. Li, J. Wang, Z. Gu, J. Lin, *Nano Lett.* **2017**, *17*, 928.
[39] B. Yu, B. Choi, W. Li, D.-H. Kim, *Nat. Commun.* **2020**, *11*, 3637.
[40] E. R. Pereira, D. Jones, K. Jung, T. P. Padera, *Semin. Cell Dev. Biol.* **2015**, *38*, 98.
[41] J. M. Ubellacker, A. Tasdogan, V. Ramesh, B. Shen, E. C. Mitchell, M. S. Martin-Sandoval, Z. Gu, M. L. McCormick, A. B. Durham, D. R. Spitz, Z. Zhao, T. P. Mathews, S. J. Morrison, *Nature* **2020**, *585*, 113.
[42] S. Kato, S. Mori, T. Kodama, *J. Cancer* **2015**, *6*, 1282.
[43] S. Cai, Y. Xie, N. M. Davies, M. S. Cohen, M. L. Forrest, *J. Pharm. Sci.* **2010**, *99*, 2664.
[44] S. Y. Seong, P. Matzinger, *Nat. Rev. Immunol.* **2004**, *4*, 469.
[45] A. Ruiz-de-Angulo, M. Bilbao-Asensio, J. Cronin, S. J. Evans, M. J. D. Clift, J. Llop, I. V. J. Feiner, R. Beadman, K. Z. Bascarán, J. C. Mareque-Rivas, *iScience* **2020**, *23*, 101499.
[46] D. J. Irvine, M. C. Hanson, K. Rakhra, T. Tokatlian, *Chem. Rev.* **2015**, *115*, 11109.
[47] D. F. Moyano, M. Goldsmith, D. J. Solfiell, D. Landesman-Milo, O. R. Miranda, D. Peer, V. M. Rotello, *J. Am. Chem. Soc.* **2012**, *134*, 3965.

[48] M. Cobaleda-Siles, M. Henriksen-Lacey, A. R. De Angulo, A. Bernecker, V. G. Vallejo, B. Szczupak, J. Llop, G. Pastor, S. Plaza-Garcia, M. Jauregui-Osoro, L. K. Meszaros, J. C. Mareque-Rivas, *Small* **2014**, *10*, 5054.
[49] A. Ruiz-de-Angulo, A. Zabaleta, V. Gómez-Vallejo, J. Llop, J. C. Mareque-Rivas, *ACS Nano* **2016**, *10*, 1602.
[50] A. I. Bocanegra Gondan, A. Ruiz-de-Angulo, A. Zabaleta, N. Gómez Blanco, B. M. Cobaleda-Siles, M. J. García-Granda, D. Padro, J. Llop, B. Arnaiz, M. Gato, D. Escors, J. C. Mareque-Rivas, *Biomaterials* **2018**, *170*, 95.
[51] G. Traini, A. Ruiz-de-Angulo, J. B. Blanco-Canosa, K. Zamacola Bascarán, A. Molinaro, A. Silipo, D. Escors, J. C. Mareque-Rivas, *Small* **2019**, *15*, 1803993.
[52] J. Hernández-Gil, M. Cobaleda-Siles, A. Zabaleta, L. Salassa, J. Calvo, J. C. Mareque-Rivas, *Adv. Healthcare Mater.* **2015**, *4*, 1034.
[53] E. Ruggiero, J. Hernández-Gil, J. C. Mareque-Rivas, L. Salassa, *Chem. Commun.* **2015**, *51*, 2091.
[54] H. Huang, Y. Dong, Y. Zhang, D. Ru, Z. Wu, J. Zhang, M. Shen, Y. Duan, Y. Sun, *Theranostics* **2019**, *9*, 1047.
[55] A. Schudel, D. M. Francis, S. N. Thomas, *Nat. Rev. Mater.* **2019**, *4*, 415.
[56] E. D. Golla, G. H. Ayres, *Talanta* **1973**, *20*, 199.
[57] A. Nemirovski, I. Vinograd, K. Takrouri, A. Mijovilovich, A. Rompel, D. Gibson, *Chem. Commun.* **2010**, *46*, 1842.
[58] J. Hernández-Gil, M. Cobaleda-Siles, A. Zabaleta, L. Salassa, J. Calvo, J. C. Mareque-Rivas, *Adv. Healthcare Mater.* **2015**, *4*, 1034.
[59] S. J. Dixon, K. M. Lemberg, M. R. Lamprecht, R. Skouta, E. M. Zaitsev, C. E. Gleason, D. N. Patel, A. J. Bauer, A. M. Cantley, W. S. Yang, B. Morrison, B. R. Stockwell, *Cell* **2012**, *149*, 1060.
[60] J. Hannemann, K. Baumann, *Toxicology* **1988**, *51*, 119.
[61] G. Barrera, *ISRN Oncol.* **2012**, *2012*, 137289.
[62] T. P. Szatrowski, C. F. Nathan, *Cancer Res.* **1991**, *51*, 794.
[63] Q. Chen, L. Feng, J. Liu, W. Zhu, Z. Dong, Y. Wu, Z. Liu, *Adv. Mater.* **2016**, *28*, 7129.
[64] Q. Chen, M. G. Espey, M. C. Krishna, J. B. Mitchell, C. P. Corpe, G. R. Buettner, E. Shaded, M. Levine, *Proc. Natl. Acad. Sci. USA* **2005**, *102*, 13604.
[65] N. Shenoy, E. Creagan, T. Witzig, M. Levine, *Cancer Cell* **2018**, *34*, 700.
[66] B. Ngo, J. M. Van Riper, L. C. Cantley, J. Yun, *Nat. Rev. Cancer* **2019**, *19*, 271.
[67] R. A. Luchtel, T. Bhagat, K. Pradhan, W. R. Jacobs, M. Levine, A. Verma, N. Shenoy, *Proc. Natl. Acad. Sci. USA* **2020**, *117*, 1666.
[68] D. Trachootham, J. Alexandre, P. Huang, *Nat. Rev. Drug Discovery* **2009**, *8*, 579.
[69] C. Lennicke, J. Rahn, R. Lichtenfels, L. A. Wessjohann, B. Seliger, *Cell Commun. Signaling* **2015**, *13*, 39.
[70] G.-Y. Liou, P. Storz, *Free Radical Res.* **2010**, *44*, 479.
[71] S. H. Dho, J. Y. Kim, E.-S. Kwon, J. C. Lim, S. S. Park, K.-S. Kwon, *Oncotarget* **2015**, *6*, 39235.
[72] G. Corna, L. Campana, E. Pignatti, A. Castiglioni, E. Tagliafico, L. Bosurgi, A. Campanella, S. Brunelli, A. A. Manfredi, P. Apostoli, L. Silvestri, C. Camaschella, P. Rovere-Querini, *Haematologica* **2010**, *95*, 1814.
[73] S. Recalcati, M. Locati, A. Marini, P. Santambrogio, F. Zaninotto, M. De Pizzol, L. Zammataro, D. Girelli, G. Cairo, *Eur. J. Immunol.* **2010**, *40*, 824.
[74] M. A. Miller, Y.-R. Zheng, S. Gadde, C. Pfirschke, H. Zope, C. Engblom, R. H. Kohler, Y. Iwamoto, K. S. Yang, B. Askevold, N. Kolishetti, M. Pittet, S. J. Lippard, O. C. Farokhzad, R. Weissleder, *Nat. Commun.* **2015**, *6*, 8692.
[75] M. Schieber, N. S. Chandel, *Curr. Biol.* **2014**, *24*, R453.
[76] J. Yun, E. Mullarky, C. Lu, K. N. Bosch, A. Kavalier, K. Rivera, J. Roper, I. I. C. Chio, E. G. Giannopoulou, C. Rago, A. Muley, J. M. Asara, J. Paik, O. Elemento, Z. Chen, D. J. Pappin, L. E. Dow, N. Papadopoulos, S. S. Gross, L. C. Cantley, *Science* **2015**, *350*, 1391.
[77] M. Lopez-Yrigoyen, L. Cassetta, J. W. Pollard, *Ann. N. Y. Acad. Sci.* **2021**, *1499*, 18.
[78] T. Muliaditan, J. Caron, M. Okesola, J. W. Opzoomer, P. Kosti, M. Georgouli, P. Gordon, S. Lall, D. M. Kuzeva, L. Pedro, J. D. Shields, C. E. Gillett, S. S. Diebold, V. Sanz-Moreno, T. Ng, E. Hoste, J. N. Arnold, *Nat. Commun.* **2018**, *9*, 2951.
[79] M. Cieslewicz, J. Tang, J. L. Yu, H. Cao, M. Zaèaljeèski, K. Motoyama, A. Lieber, E. W. Raines, S. H. Pun, *Proc. Natl. Acad. Sci. USA* **2013**, *110*, 15919.
[80] Y. Wang, Y. X. Lin, S. L. Qiao, H. W. An, Y. Ma, Z. Y. Qiao, R. P. Y. J. Rajapaksha, H. Wang, *Biomaterials* **2017**, *112*, 153.
[81] C. B. Rodell, S. P. Arlauckas, M. F. Cuccarese, C. S. Garris, R. Li, M. S. Ahmed, R. H. Kohler, M. J. Pittet, R. Weissleder, *Nat. Biomed. Eng.* **2018**, *2*, 578.
[82] T. Liang, R. Zhang, X. Liu, Q. Ding, S. Wu, C. Li, Y. Lin, Y. Ye, Z. Zhong, M. Zhou, *Int. J. Nanomed.* **2021**, *16*, 2703.
[83] Y. Qi, X. Yan, T. Xia, S. Liu, *Mater. Des.* **2021**, *198*, 109388.
[84] F. O. Martinez, S. Gordon, *F1000Prime Rep.* **2014**, *6*, 13.
[85] A. Mantovani, A. Sica, S. Sozzani, P. Allavena, A. Vecchi, M. Locati, *Trends Immunol.* **2004**, *25*, 677.
[86] Y. Chen, Y. Song, W. Du, L. Gong, H. Chang, Z. Zou, *J. Biomed. Sci.* **2019**, *26*, 78.
[87] P. Jeannin, L. Paolini, C. Adam, Y. Delneste, *FEBS J.* **2018**, *285*, 680.
[88] I. C. Arnold, S. Mathisen, J. Schulthess, C. Danne, A. N. Hegazy, F. Powrie, *Mucosal Immunol.* **2016**, *9*, 352.
[89] M. Sachet, Y. Y. Liang, R. Oehler, *Apoptosis* **2017**, *22*, 1189.
[90] P. Loke, J. P. Allison, *Proc. Natl. Acad. Sci. USA* **2003**, *100*, 5336.
[91] A. Mantovani, F. Marchesi, A. Malesci, L. Laghi, P. Allavena, *Nat. Rev. Clin. Oncol.* **2017**, *14*, 399.
[92] B. Z. Qian, J. W. Pollard, *Cell* **2010**, *141*, 39.
[93] M. De Palma, C. E. Lewis, *Cancer Cell* **2013**, *23*, 277.
[94] H. Y. Tan, N. Wang, S. Li, M. Hong, X. Wang, Y. Feng, *Oxid. Med. Cell. Longevity* **2016**, *2016*, 2795090.
[95] S. A. Stacker, S. P. Williams, T. Karnezis, R. Shayan, S. B. Fox, M. G. Achen, *Nat. Rev. Cancer* **2014**, *14*, 159.
[96] J. D. Shields, M. Borsetti, H. Rigby, S. J. Harper, P. S. Mortimer, J. R. Levick, A. Orlando, D. O. Bates, *Br. J. Cancer* **2004**, *90*, 693.
[97] J. Landsberg, J. Kohlmeyer, M. Renn, T. Bald, M. Rogava, M. Cron, M. Fatho, V. Lennerz, T. Wölfel, M. Hölzel, T. Tüting, *Nature* **2012**, *490*, 412.
[98] J. Tsoi, L. Robert, K. Paraiso, C. Galvan, K. M. Sheu, J. Lay, D. J. L. Wong, M. Atefi, R. Shirazi, X. Wang, D. Braas, C. S. Grasso, N. Palaskas, A. Ribas, T. G. Graeber, *Cancer Cell* **2018**, *33*, 890.
[99] H. Yang, Q. Wang, Z. Li, F. Li, D. Wu, M. Fan, A. Zheng, B. Huang, L. Gan, Y. Zhao, X. Yang, *Nano Lett.* **2018**, *18*, 7909.
[100] M. R. Kano, Y. Bae, C. Iwata, Y. Morishita, M. Yashiro, M. Oka, T. Fujii, A. Komuro, K. Kiyono, M. Kaminishi, K. Hirakawa, Y. Ouchi, N. Nishiyama, K. Kataoka, K. Miyazono, *Proc. Natl. Acad. Sci. USA* **2007**, *104*, 3460.
[101] J. Chen, Z. Y. Ding, S. Li, S. Liu, C. Xiao, Z. Li, B. X. Zhang, X. P. Chen, X. Yang, *Theranostics* **2021**, *11*, 1345.
[102] E. Batlle, J. Massagué, *Immunity* **2019**, *50*, 924.
[103] M. Perše, *Biomedicines* **2021**, *9*, 1406.
[104] C. He, D. Liu, W. Lin, *Biomaterials* **2015**, *36*, 124.
[105] X. Xu, K. Xie, X. Q. Zhang, E. M. Pridgen, G. Y. Park, D. S. Cui, J. Shi, J. Wu, P. W. Kantoff, S. J. Lippard, R. Langer, G. C. Walker, O. C. Farokhzad, *Proc. Natl. Acad. Sci. USA* **2013**, *110*, 18638.
[106] Y. Zhang, Y. Dong, H. Fu, H. Huang, Z. Wu, M. Zhao, X. Yang, Q. Guo, Y. Duan, Y. Sun, *Biomaterials* **2021**, *269*, 120478.
[107] T. Hadi, C. Ramseyer, T. Gautier, P. S. Bellaye, T. Lopez, A. Schmitt, S. Foley, S. Yesylevskyy, T. Minervini, R. Douhard, L. Proukhnitzky,

S. Messaoudi, M. Wendremaire, M. Moreau, F. Neiers, B. Collin, F. Denat, L. Lagrost, C. Garrido, F. Liruss, *JCI Insight* **2020**, *5*, e140280.
[108] A. B. Nair, S. Jacob, *J. Basic Clin. Pharm.* **2016**, *7*, 27.
[109] B. J. Corden, R. L. Fine, R. F. Ozols, J. M. Collins, *Cancer Chemother. Pharmacol.* **1985**, *14*, 38.
[110] S. Dhar, W. L. Daniel, D. A. Giljohann, C. A. Mirkin, S. J. Lippard, *J. Am. Chem. Soc.* **2009**, *131*, 14652.
[111] S. H. Sun, H. Zeng, D. B. Robinson, S. Raoux, P. M. Rice, S. X. Wang, G. X. Li, *J. Am. Chem. Soc.* **2004**, *126*, 273.
[112] O. Carion, B. Mahler, T. Pons, B. Dubertret, *Nat. Protoc.* **2007**, *2*, 2383.
[113] J. W. Opzoomer, J. E. Anstee, I. Dean, E. J. Hill, I. Bouybayoune, J. Caron, T. Muliaditan, P. Gordon, D. Sosnowska, R. Nuamah, S. E. Pinder, T. Ng, F. Dazzi, S. Kordasti, D. R. Withers, T. Lawrence, J. N. Arnold, *Sci. Adv.* **2021**, *7*, 9518.
[114] M. R. Hussein, *Int. J. Exp. Pathol.* **2006**, *87*, 163.
[115] C. L. Gauci, P. Alexander, *Cancer Lett.* **1975**, *1*, 29.
[116] M. Cobaleda-Siles, M. Henriksen-Lacey, A. R. de Angulo, A. Bernecker, V. G. Vallejo, B. Szczupak, J. Llop, G. Pastor, S. Plaza-Garcia, M. Jauregui-Osoro, L. K. Meszaros, J. C. Mareque-Rivas, *Small* **2014**, *10*, 5053.
[117] V. Ščasnár, J. E. van Lier, *Eur. J. Nucl. Med.* **1993**, *20*, 273.